Effect of Aminoalcohols on Morphology of Nanocrystalline ZnO Powders and Its Optical Properties

Kanokwan Thongsuriwong

A Thesis Submitted in Partial Fulfillment of the Requirements

for the Degree of Master of Science in Chemical Studies

Prince of Songkla University

2009

Copyright of Prince of Songkla University

Thesis Title   Effect of Aminoalcohols on Morphology of Nanocrystalline

        ZnO Powders and Its Optical Properties

Author   Miss Kanokwan Thongsuriwong

Major Program Chemical Studies

Major Advisor   **Examining Committee**

…………………………………... ………………………..Chairperson

(Dr. Pongsaton Amornpitoksuk) (Dr. Tanakorn Ratana)

           …………………………………......

Co-advisor   (Dr. Pongsaton Amornpitoksuk)

………………………………….... …………………………………......

(Asst. Prof. Dr. Sumetha Suwanboon) (Asst. Prof. Dr. Sumetha Suwanboon)

           …………………………………......

           (Dr. Nararak Leesakul)

    The Graduate School, Prince of Songkla University, has approved this thesis as partial fulfillment of the requirements for the Master of Science Degree in Chemical Studies.

            …………………………………..

            (Assoc. Prof. Dr. Krerkchai Thongnoo)

             Dean of Graduate School

ชื่อวิทยานิพนธ์	อิทธิพลของอะมิโนแอลกอฮอล์ต่อลักษณะทางสัณฐานของผงซิงค์ออก
	ไซด์ที่มีขนาดผลึกในระดับนาโนเมตรและสมบัติเชิงแสง
ผู้เขียน	นางสาวกนกวรรณ ทองสุริวงศ์
สาขาวิชา	เคมีศึกษา
ปีการศึกษา	2551

บทคัดย่อ

งานวิจัยนี้ได้ศึกษาอิทธิพลของสารเพิ่มความเสถียรในกลุ่มอะมิโนแอลกอฮอล์ ได้แก่ โมโนเอทาโนลามีน ไดเอทาโนลามีน และไตรเอทาโนลามีน ต่อลักษณะทางสัณฐานของอนุภาคซิงค์ออกไซด์ ผลการทดลองพบว่าขนาดผลึก และขนาดอนุภาคมีค่าลดลงเมื่อความเข้มข้นของอะมิโนแอลกอฮอล์เพิ่มขึ้น เนื่องจากการยับยั้งการเติบโตของผลึกซิงค์ออกไซด์ในแนวแกนซี ในการศึกษานี้พบว่าไตรเอทาโนลามีนจะส่งผลต่อสัณฐานของอนุภาคซิงค์ออกไซด์มากที่สุด เมื่อเปรียบเทียบกับโมโนเอทาโนลามีน และไดเอทาโนลามีน เนื่องจากผลทางสเตอริก เมื่อวัดค่าการส่องผ่านของแสงของอนุภาคซิงค์ออกไซด์ที่ผ่านการเผาแคลไซน์แล้วพบว่าผงซิงค์ออกไซด์ให้ค่าการส่องผ่านสูงในช่วงวิสิเบิล คุณลักษณะในการเปล่งแสง และความเข้มของการเปล่งแสงของผงซิงค์ออกไซด์ เมื่อศึกษาด้วยเครื่องโฟโตลูมิเนสเซนซ์ สเปกโตรโฟโตมิเตอร์ ที่อุณภูมิห้อง พบแถบการเปล่งแสงในช่วงอัลตร้าไวโอเลตที่มีความเข้มสูงสุดที่ 390 นาโนเมตร นอกจากนี้ได้ทำการศึกษาสมบัติการเป็นโฟโตคะตะลิสต์ในสารละลายเมทิลีนบลู ผลการทดสอบพบว่า ผงซิงค์-ออกไซด์ที่เตรียมได้จากการเติมสารเพิ่มความเสถียรในกลุ่มอะมิโนแอลกอฮอล์มีประสิทธิภาพในการเป็นโฟโตคะตะลิสต์น้อยกว่าผงซิงค์ออกไซด์ที่ไม่มีการเติมสารเพิ่มความเสถียร

Thesis Title   Effect of Aminoalcohols on Morphology of Nanocrystalline ZnO Powders and Its Optical Properties

Author   Miss Kanokwan Thongsuriwong

Major Program   Chemical Studied

Academic Year   2009

ABSTRACT

The potential of aminoalcohol (monoethanolamine (MEA), diethanolamine (DEA) and triethanolamine (TEA)) on morphological control of ZnO particles has been investigated in this study. The crystallite and particle size decrease as increasing the aminoalcohol concentration owing to the inhibition of the crystal growth of ZnO along c-axis. TEA affects mostly the ZnO morphology comparing to MEA and DEA due to its steric effect. The optical transmittance spectrum of all calcined ZnO powders show a highly transparent mode in visible region. The emission characteristic and the emission intensity of nanocrystalline ZnO powders investigated by photoluminescence spectrometer at room temperature show a strong UV band emission centered at 390 nm. Moreover, the photocatalytic degradation of methylene blue (MB) was also studied. It has been found that the aminoalcohol modified-ZnO powders have lower photocatalytic efficiency than that prepared ZnO without aminoalcohol.

ACKNOWLEDGEMENT

CONTENTS

CONTENTS (CONTINUED)

LIST OF TABLES

LIST OF FIGURES

CHAPTER 1

INTRODUCTION

1. Nanomaterials

Nanotechnology is a collective definition referring to design, characterization, production and application of structures, devices and systems by controlling shape and size at nanometer scale. The prefix "nano" which is derived from the Greek word for dwarf, means a one thousand millionth of a meter 10^{-9}. Generally, nanomaterials have structured components with at least one dimension less than 100 nm (Holister, *et al*., 2003).

Nanostructures can be classified into three groups depending upon the confinement of particles in a particular crystallographic direction within a structure. The three groups are (Cao, 2004):

1. Zero-dimensional (0D) nanostructure: the materials that confine electrons in three dimensions or the structure does not permit free particle motion in any direction. Semiconductor quantum dots, nanoparticles and colloidal particles are some examples to include in this group.

2. One-dimensional (1D) nanostructure: the materials that confine electrons in two dimensions or the structure does not permit free particle motion in two dimensions. Some examples are nanorods, nanowires, nanotubes and nanofilaments etc.

3. Two-dimensional (2D) nanostructure: the materials exhibit a confinement of electrons in one dimension or the structure does not permit free particle motion in one dimension, such as nano discs or platelets, thin film on a surface and multilayered material.

(a)

(Chen, C. *et al*., 2008)

(Gupta, A. *et al*., 2006)

(b)

(Pal and Santiago, 2005)

(Kim, G.-S. *et al*., 2007)

(c)

(Lee, J.-H. *et al*., 2003)

(Tsay, C.-Y. *et al*., 2008)
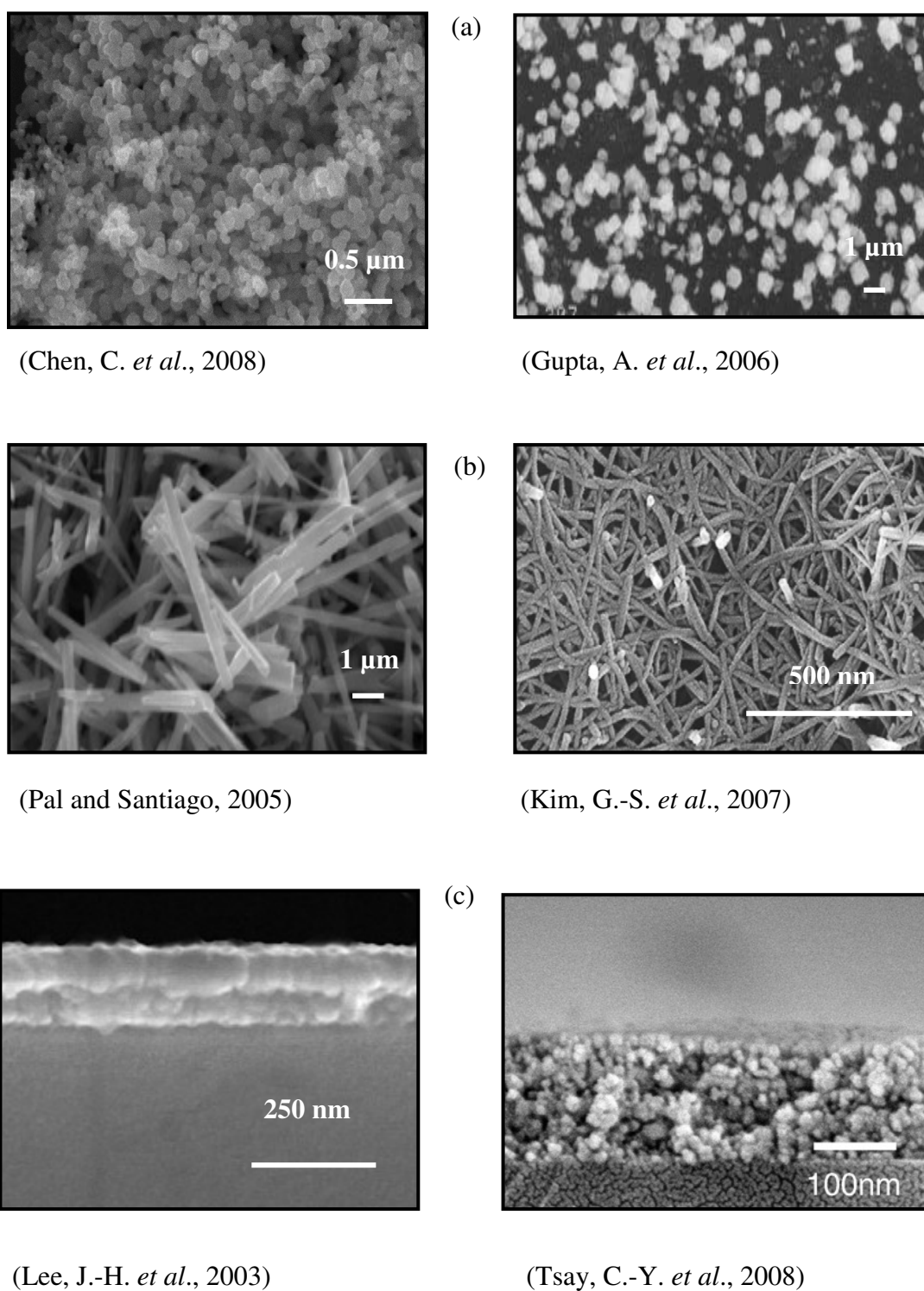
Figure 1. Examples of (a) zero-dimentional (0D), (b) one-dimentional (1D) and (c) two-dimentional (2D) nanostructures.

2. General description of ZnO

As far as nanomaterial is concerned, ZnO is one of the candidate which has been attracting attention due to its numerous interested properties.

Zinc oxide is a chemical compound with the formula ZnO. It is produced by two main different processes. In the direct or American method, zinc ores (or residues) are heated in air with coke or anthracite, and the resulting zinc vapour is subjected to controlled oxidation. In the indirect or French method, the zinc vapour to be oxidized is obtained by boiling zinc (http://en.wikipedia.org/wiki/zinc-oxide).

ZnO is nearly insoluble in acids and bases. It characterizes as white powder commonly known as zinc white. It occurs in nature as the mineral zincite. Crystalline ZnO exhibits the piezoelectric effect and ZnO performs a thermochrome characteristic by changing from white to yellow when heating, and vice versa. The ZnO has been widely studied since 1935. ZnO is a well-known semiconductor with a wide direct band gap (3.37 eV) and large exciton binding energy of about 60 meV at room temperature (http://en.wikipedia.org/wiki/zinc-oxide).

ZnO powder has been commonly used for over a hundred years in a wide range of applications, for example,

1. Medical applications

A mixture of ZnO and 0.5% Fe_2O_3 (calamine) is used in calamine lotion and a mixture of ZnO and eugenol (zinc oxide eugenol) has restorative and prosthodontic applications in dentistry (http://en.wikipedia.org/wiki/zinc-oxide). Moreover, the ZnO nanopowders can use as antimicrobial agent (Mungkornasawakul, *et al.*, 2005).

2. Food additive

ZnO is added to many breakfast cereals acting as a source of zinc that is a necessary nutrient for ZnO based medicament for preventing and treating diarrhea in farm animals (http://www.freepatentsonline.com/EP1593381.html). (http://en.wikipedia.org/wiki/zinc-oxide).

3. Pigment

Over the past century, the paint industry (in its constant development of improved products) has utilized various aspects of those properties to high degree. Manufacturers discovered that they could produce the coatings of brushing consistency and good suspension properties by incorporation of ZnO into their pastes.

Zinc white is used as a pigment in paints. In general, zinc white is more opaque than lithopone, but it is less opaque than titanium dioxide. It is also used in coating for paper. Chinese white is a special grade of zinc white used in artists' pigments, because it can absorb both UVA and UVB rays of ultraviolet light. Interestingly, the current state-of-the-art thermal control coatings (TCCs) system utilizes ZnO pigment to maintain solar reflectance over a long exposure time (http://cat.inist.fr/?aModele=afficheN&cpsidt=15369294).

4. Cosmetic applications

ZnO is applied in cosmatics to protect the UV radiation for human (Samontha, *et al*). ZnO can be used in ointments, creams, and lotions to protect against sunburn and other damages to the skin caused by ultraviolet light. It is the broadest spectrum UVA and UVB absorber that is approved for use as a sunscreen by the Food and Drug Administration (FDA), and is completely photostable and it is also a main ingredient of mineral make up (http://www.goldbamboo.com/topic-t4989-a1-6Zinc_Oxide.html).

5. Rubber manufacture

ZnO proved the most effective activator to speed up the rate of cure with the new accelerators. It provides reinforcement in natural rubber, and in some synthetic elastomers such as polysulfides and chloroprenes. The degree of reinforcement depends upon a combination of the particle size, the finest size being the most effective. ZnO is the chemical reactivity that utilized to activate the organic accelerator. The unreacted portion of ZnO remains available as a basic reserve to neutralize the sulfur-bearing acidic decomposition products formed during vulcanization. Adequate levels of ZnO contribute markedly to chemical reinforcement, scorch control, resistance to heat-aging and compression fatigue. Additional ZnO also provides heat conduction to more rapidly dissipate the heat and thereby provides lower operating temperatures. In addition, it imparts heat

stabilization by reacting with acidic decomposition products (http://navbharat.co.in/clients.htm).

6. Plastic applications

Zinc compounds can provide a variety of properties in the plastic field. Heat resistance and mechanical strength are imparted to acrylic composites by ZnO. Addition of ZnO to epoxy resins cured with aliphatic polyamines imparts higher tensile strength and water resistance. ZnO is also useful in the preparation of nylon polymers and in increasing their resistance and reacts with unsaturated polyesters to form higher viscosity and a thixotropic body. ZnO increases the transparency of poly (chlorofluoro ethylene) molding resin. Polyolefin's are improved in color, tensile strength, and vulcanization properties by addition of ZnO. Applications in development for zinc oxide-stabilized polypropylene and high-density polyethylene include safety helmets, stadium seating, insulation, pallets, bags, fiber and filament, agricultural and recreational equipment (http://navbharat.co.in/clients.htm).

7. Electronic applications

The most common applications of ZnO are in laser diodes and light emitting diodes (LEDs) since it has an exciton and biexciton energies of 60 meV and 15 meV, respectively. Additional it is inexpensive. Most ZnO has an n-type character even in the absence of intentional doping. The native defects such as oxygen vacancies or zinc interstitials are often assumed to be the origin of this, but the subject remains controversial. The n-type doped films are often used in thin film technology, where ZnO serves as a transparent conducting oxide (TCO). The n-type doping is possible by introduction of group III elements such as Al, Ga or In. These group III elements can generate the donor state near the conduction band and they can generate the excess electrons at the bottom of conduction band. On the contrary, it is difficult to dope ZnO as p-type semiconductor due to the high activation energy of acceptor, low solubility of acceptor dopants and self-compensating process on acceptor doping caused by intrinsic defects. Recently, the strategy of p-type ZnO semiconductor is an active area of research. Thin-film solar cells, liquid crystal display (LCD) and flat panel displays are typical applications of p-type ZnO semiconductor material. Appropriately doped ZnO may be transparent and conductive, and they can therefore be used as a transparent conducting oxide in some important devices in place of

indium doped tin oxide (ITO) material. Beside, conducting ZnO material is a good infrared reflectors and can be used as energy efficent windows that require high reflective index and high transmittance in the visible range. (http://www.eurekalert/pab.releases/2007.01/uoc--clfo10207.html) (http://en.wikipedia.org/wiki/zinc-oxide)

8. Sensor applications

ZnO can use for pyroelectric sensors. It possesses the advantages of being integrable with on-chip circuitry, un-cooled detecting, room-temperature operation, fast and wide spectral response with high sensitivity and low cost (Hsiao *et al*., 2008).

ZnO material can be used in sensing and/or monitoring different types of gases both toxic and harmful gases as chlorine (Cl_2) due to it low cost, high sensitivity, excellent selectivity quick response behavior, sulfur hexafluoride, butane ethanol and gasoline (Majumder *et al*., 2003; Xu et al., 2000; Xinshu *et al*., 2004).

3. Crystallographic data of ZnO

ZnO exists in three forms depending on pressure. At ambient pressure, ZnO is in the stable hexagonal wurtzite (ZnO_W) form and some ZnO is in the metastable cubic zinc-blend (ZnO_{ZB}) form. At moderate and high pressure (8-10 GPa), ZnO is in the rock-salt (ZnO_{RS}) form. The difference between the critical pressure for the ZnO_{ZB} to ZnO_{RS} and ZnO_W to ZnO_{RS} transition is very small and so the energy difference between ZnO_W and ZnO_{RS} is also very small. Thus, the ZnO_W to ZnO_{RS} transition can occur due to the topotactic transformation based on the network of oxygen and zinc (Qteish, 2000; Serrano *et al*., 2004)

At ambient pressure and temperature, ZnO crystallizes in the wurtzite (*B4* type) structure whose underlying Bravais lattice in hexagonal (space group *P6₃ mc* = C^4_{6v}). The structure of ZnO is illustrated in figure 2. Under ambient condition, its lattice parameters are *a* = 3.2489 (1) Å and *c* = 5.2053 (4) Å. Both kinds of atoms are located in Wyckoff position:

$$2(b) = \quad \frac{1}{3}\frac{2}{3}v, \quad \frac{2}{3}\frac{1}{3}\,v + \frac{1}{2}$$

and the arrangements are in the positions:

$$\text{Zn: } 000, \quad \frac{1}{3}\frac{2}{3}\frac{1}{2}$$

$$\text{O: } 00u, \quad \frac{1}{3}\frac{2}{3}u + \frac{1}{2}$$

In an ideal wurtzite crystal, the axial ratio $c/a = (8/3)^{1/2}$ and $u = 3/8$. Experimentally, the real values of u and c/a of wurtzite ZnO were, however, determined in the range of $u = 0.3817$ to 0.3856 and $c/a = 1.593$ to 1.6035.
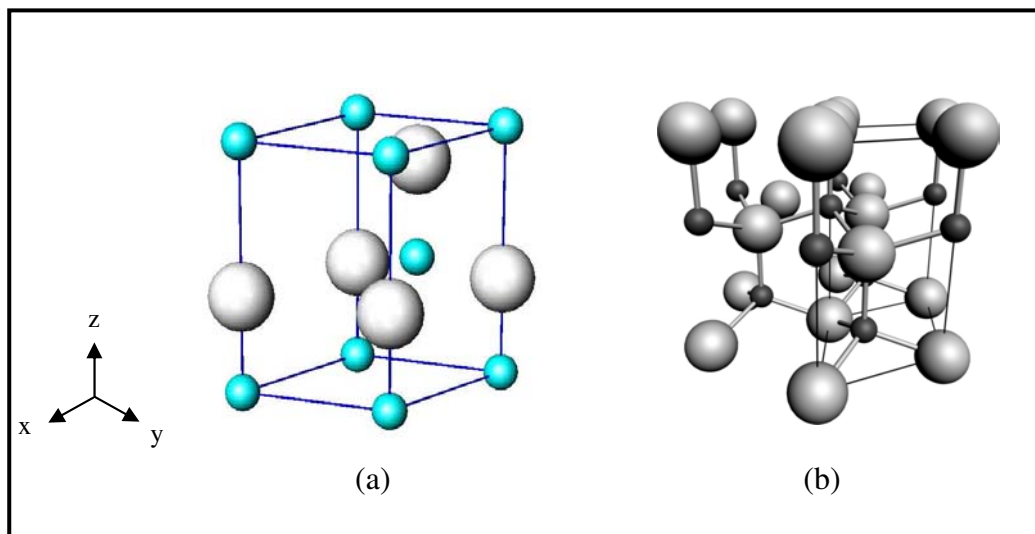
Figure 2. A drawing shows; (a) unit cell of ZnO and (b) tetrahedral coordination in
ZnO. Big and small spheres represent oxygen and zinc atoms, respectively.
Source: http://www.geocities.jp/ohba_lab_ob_page/Structure/ZnO_Wurtzite.jpg
Source: Jagadish and Pearton (2006)

ZnO wurtzite structure is characterized by tetrahedral coordination of ion of one kind (e.g. Zn^{2+}) by the ions of another kind (e.g. O^{2-}) as composed of ZnO_4, or OZn_4, tetrahedral (Figure 2b). They are stacked in a hexagonal close-packed array with the tetrahedral edges of alternate layers rotated through 180° around the c-axis. The tetrahedral coordination of this compound is also a common indicator of sp^3 covalent bonding (the Zn d-electrons hybidrize with the O p-electrons). However, the bonding between the Zn atoms and O atoms are highly ionic, due to the large difference in their electronegative values (1.65 for Zn and 3.44 for O) thus ZnO lies on the borderline between being classed as a covalent and ionic compound.

4. Review of literatures

Lee *et al*., (2003) investigated the effect of drying conditions and heat treatment process on the structural, electrical and optical properties of ZnO thin films prepared by sol–gel method. The precursor solution was prepared by mixing zinc acetate dihydrate and monoethanolamine (MEA) in 2-methoxyethanol. The molar ratio of MEA to zinc acetate was kept constant at 1.0. ZnO films that were dried at 350°C and then heated at 600°C showed an extremely sharp (002) peak in the XRD pattern. The films were more oriented preferentially along (002) direction, the greater their electrical and optical properties became. By applying the second-heat treatment in nitrogen with 5% hydrogen at 500°C, the grain size of the films was increased, the resistivity value was 0.099 Ω.cm and optical transmittance was higher than 85% in the visible range.

Li *et al.,* (2004, 2005) investigated the effect of annealing temperature on microstructure, morphology and transparency of ZnO thin film prepared by spin coating on silica glass substrate. Figure 3 shows the flow chart for preparation of ZnO thin film via sol-gel method. By using 2-methoxyethanol and monoethanolamine (MEA) as a solvent and stabilizer, respectively, the peak intensity of (002) plane and the average transmittance of the prepared film increased as annealing temperature was increased from 400 to 600°C. Furthermore, the hexagonal grain became larger and the film strongly oriented along the c-axis at annealing temperature of 600°C.
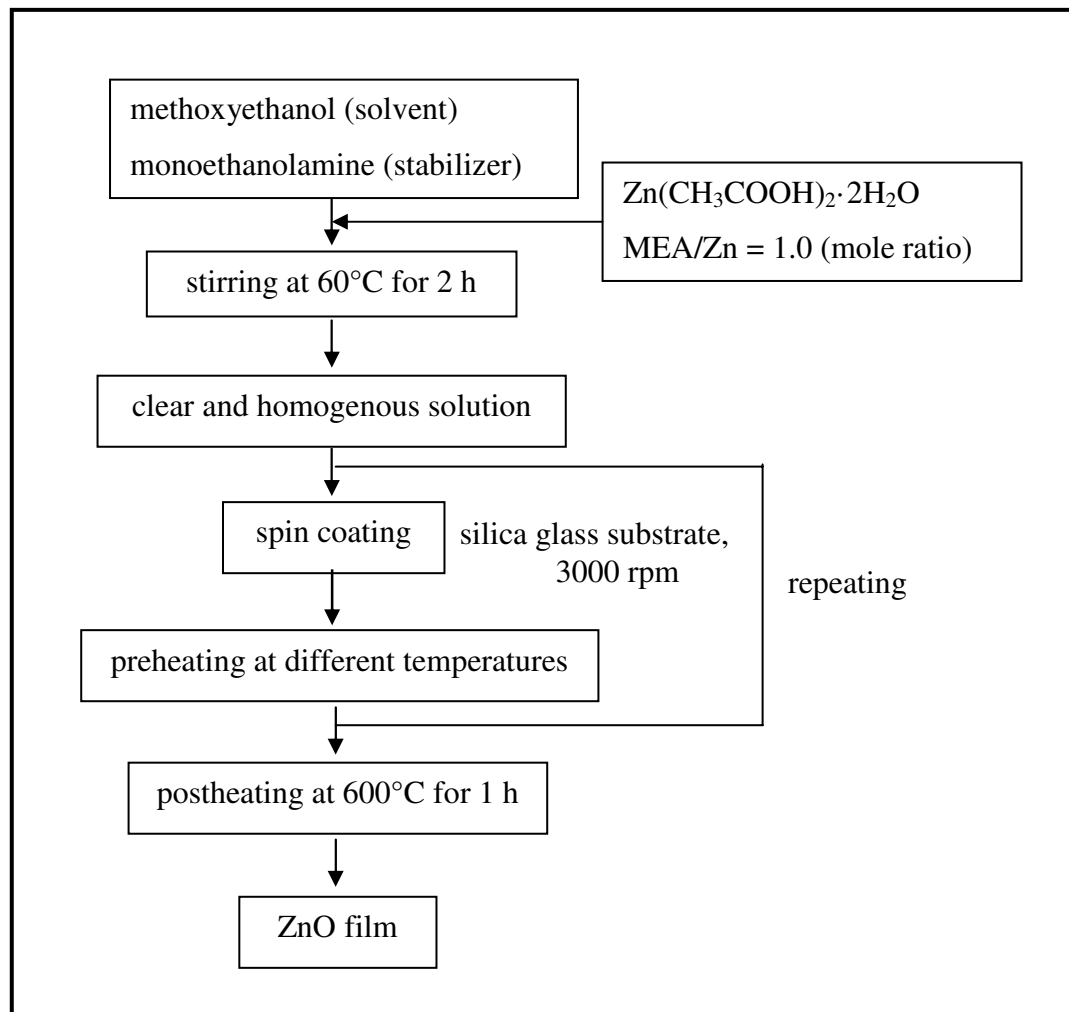
Figure 3. The flow chart shows the procedure for preparing ZnO films.

Source: Li *et al.,* (2004)

Sagar *et al.,* (2007) studied the influence of pH value on the quality of ZnO film using monoethanolamine (MEA) as a stabilizer in methanol. The increase in pH value of the sols resulted in the growth of ZnO film, smooth microstructure, large grain size and low surface roughness. They reported that high quality of ZnO films was obtained by using the sol with the molar ratio of MEA to zinc acetate of 1:1 and pH value of 10.6.

O'Brien *et al.,* (2007) prepared the ZnO thin film on fused silica glass by single spin coating from precursor sol prepared from monoethanolamine (MEA) and isopropanol that act as stabilizer and solvent, respectively. The molar ratio of

MEA to zinc acetate was maintained at 1.0. The degree of *c*-axis orientation of prepared ZnO thin films was strongly dependent on the initial zinc concentration. An increase of zinc concentration to 1.3 M resulted in a film preferentially oriented in the (101) plane. The average crystallite size and film thickness were increased with increasing the zinc concentration up to 0.7 M. The transmittance of films was 80-92% in visible region and the optical band gap energy was in the range of 3.298-3.306 eV. Photoluminescence showed a strong emission centered at *ca*. 380 nm along with a broad yellow-orange emission centered at *ca*. 610 nm.

Winfiel *et al.,* (2007) used monoethanolamine (MEA) as a stabilizer to prepare the ZnO thin film on soda-lime glass by a single spin coating method. The molar ratio of MEA to zinc acetate was kept constant at 1.0. After the sample was irradiated by an excimer laser, the hexagonal ZnO wurtzite structure was observed in XRD pattern. The films had a transparency over 70% in the visible and the optical band gap energy was about 3.454 eV. After laser irradiation, the surface roughness of ZnO thin film increased from 2.43 to 11.03 nm that differed significantly from ZnO sol-gel films annealed in conventional furnace.

Yu *et al.,* (2007) investigated the effect of pH value on shape alteration of ZnO nanocrystal arrays. Firstly, ZnO thin films were prepared from the seed solution that the molar ratio of MEA to zinc acetate was 1:1 in 2-methoxyethanol by sol-gel dip coating on ITO glass substrates. The substrates covering with a seed layer were immersed in mixed solution between $Zn(NO_3)_2 \cdot 6H_2O$ and ammonia solution at different pH values. From their study, if the zinc concentration was varied from 0.04 to 0.1 M, the suitable pH values for the heterogeneous nucleation was in a range of 8.5-9.5. When the pH values was raised, the average diameter of ZnO nanorods varied from ~ 50 to 170 nm and the length was longer than that of the particles obtained at lower pH value. Nanorod shape could be transformed by secondary pH adjustment. If the pH value of solution was increased, the central part of nanorods was mainly eroded and nanotubes were shaped. Furthermore, the side plan could split if the erosion occurred for a long time and then the nanosheets appeared (Figure 4). On the contrary, if the pH value of solution was decreased, the small particles bestrewed the surfaces of the nanotube and the blanket-like shaped surface was fabricated (Figure 5).
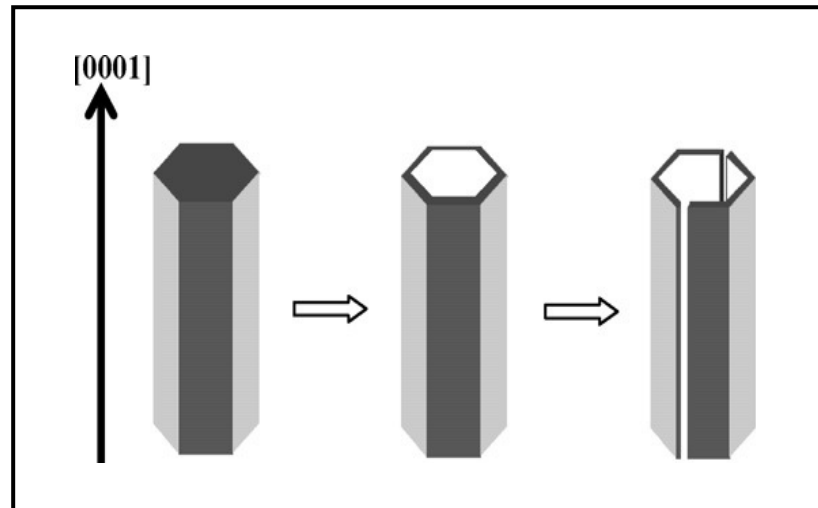
Figure 4. The formation process of ZnO nanotubes and nanosheets.
Source: Yu *et al.,* (2007)
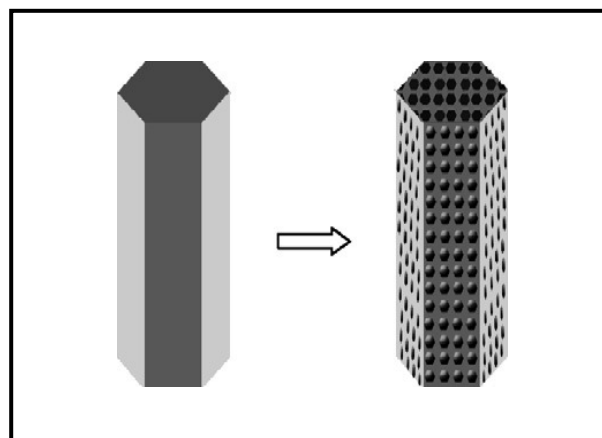
Figure 5. The formation process of ZnO rods with blanket-like shaped surface.
Source: Yu *et al.,* (2007)

Yahia *et al.,* (2008) prepared the ZnO thin film with a preferred (002) orientation by sol-gel method as $Zn(CH_3COOH)_2 \cdot 2H_2O$ and ethanol were used as a starting material and solvent, respectively. A stable solution was prepared at molar ratio of $[MEA]/[Zn^{2+}] = 2$. The precursor solution was dropped and deposited on glass substrates by spin-coating (3,000 rmp; 10 s). After thermal annealing, the film

crystallinity and *c*-axis orientation were improved by decreasing concentration of the precursor from 2 M to 0.75 M. The films consisted of spongy particles aggregated with an uniform size and homogeneous surface. The Raman spectroscopy of zinc acetate dihydrate has been performed to study the chemical entities evolution from the state of solution to the state of film. The Raman investigation of the deposit solution proved that Zn-O bonds played probably the role in the initation crystallization during the heat treatment of the films.

Hwangbo *et al*., (2008) investigated the photoluminescence characteristic of an amorphous ZnO thin film on soda-lime-silica glass substrate prepared by sol-gel method at low temperature. A homogeneous coating solution was prepared by mixing zinc acetate dihydrate ($Zn(CH_3COOH)_2 \cdot 2H_2O$) and monoethanolamine (MEA) in 2-methoxyethanol ($HOCH_2CH_2OCH_3$). The molar ratio of MEA to zinc acetate was fixed at 1.0. After coating process, the samples were dried in air at 100°C for 60 min. The dried film showed an amorphous characteristic in XRD pattern. The photoluminescence spectrum of ZnO thin film with an intense near band edge emission was observed while the defect-related broad green emission was nearly quenched.

Raoufi and Raoufi (2009) prepared ZnO thin films by sol-gel method. The flow chart of preparation is shown in figure 6. XRD analysis revealed that the annealed ZnO thin films consisted of a single phase ZnO with wurtzite structure and the films showed the *c*-axis orientation. The quality of prepared films and their crystallization were more influenced by heating temperature than heating time. The relative intensity of peak corresponding to the (002) plane and crystallite size of the film increased with increasing the annealing temperature. The annealed films were highly transparent with average transmission exceeding 80% in the visible region (400-700 nm). The measured optical band gap values of ZnO thin films were between 3.26 eV and 3.28 eV, which were in the range of band gap values of intrinsic ZnO (3.2–3.3 eV). SEM analysis of annealed thin films displayed a completely different surface morphology. The surface of the annealed thin film at 300°C contained some cracks while no crack was observed after annealing at 400°C and 500°C.
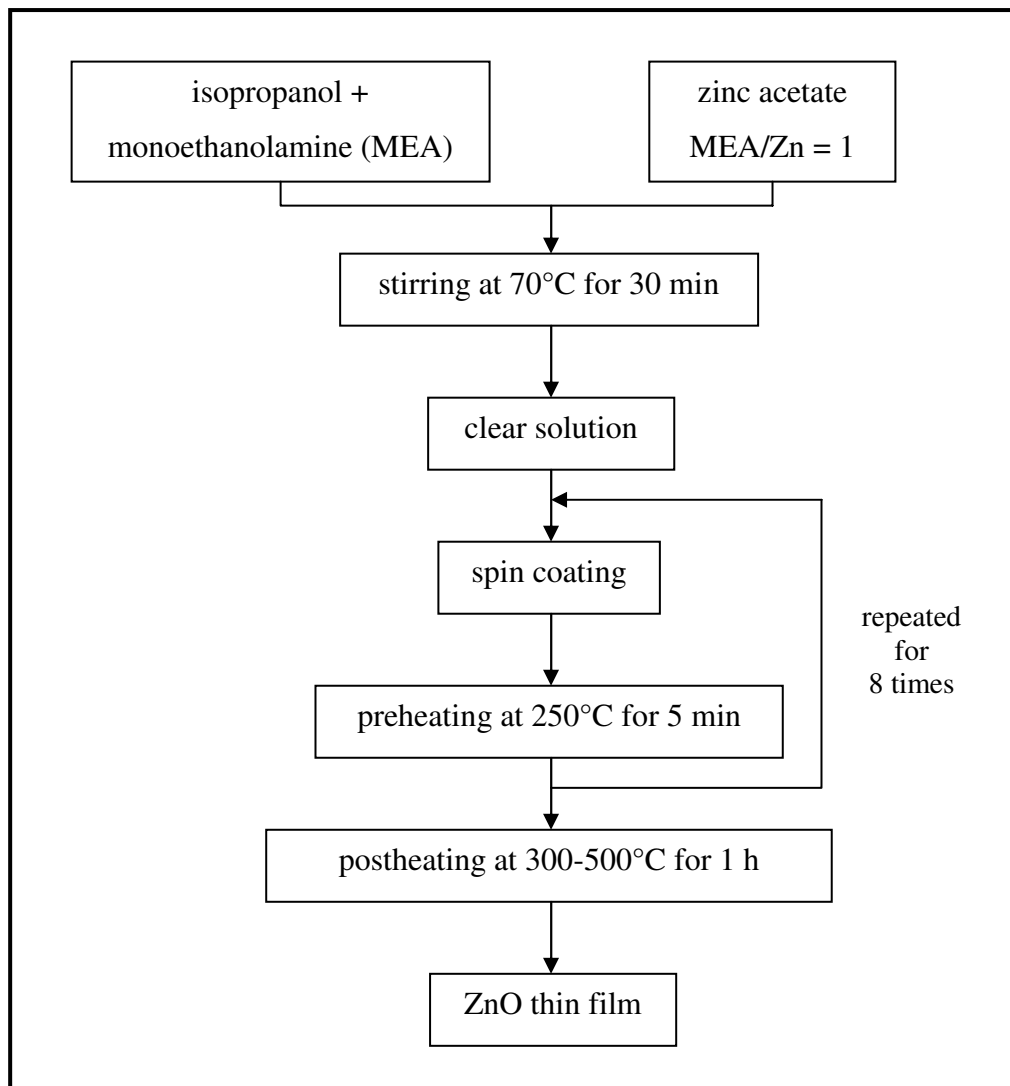
Figure 6. Flow chart of sol-gel method for preparation of ZnO thin film.

Source: Raoufi and Raoufi (2009)

Caglar *et al.,* (2009) investigated the electrical conductivity and optical properties of nanostructured ZnO thin film prepared by sol–gel spin coating method on glass substrate as shown in figure 7.
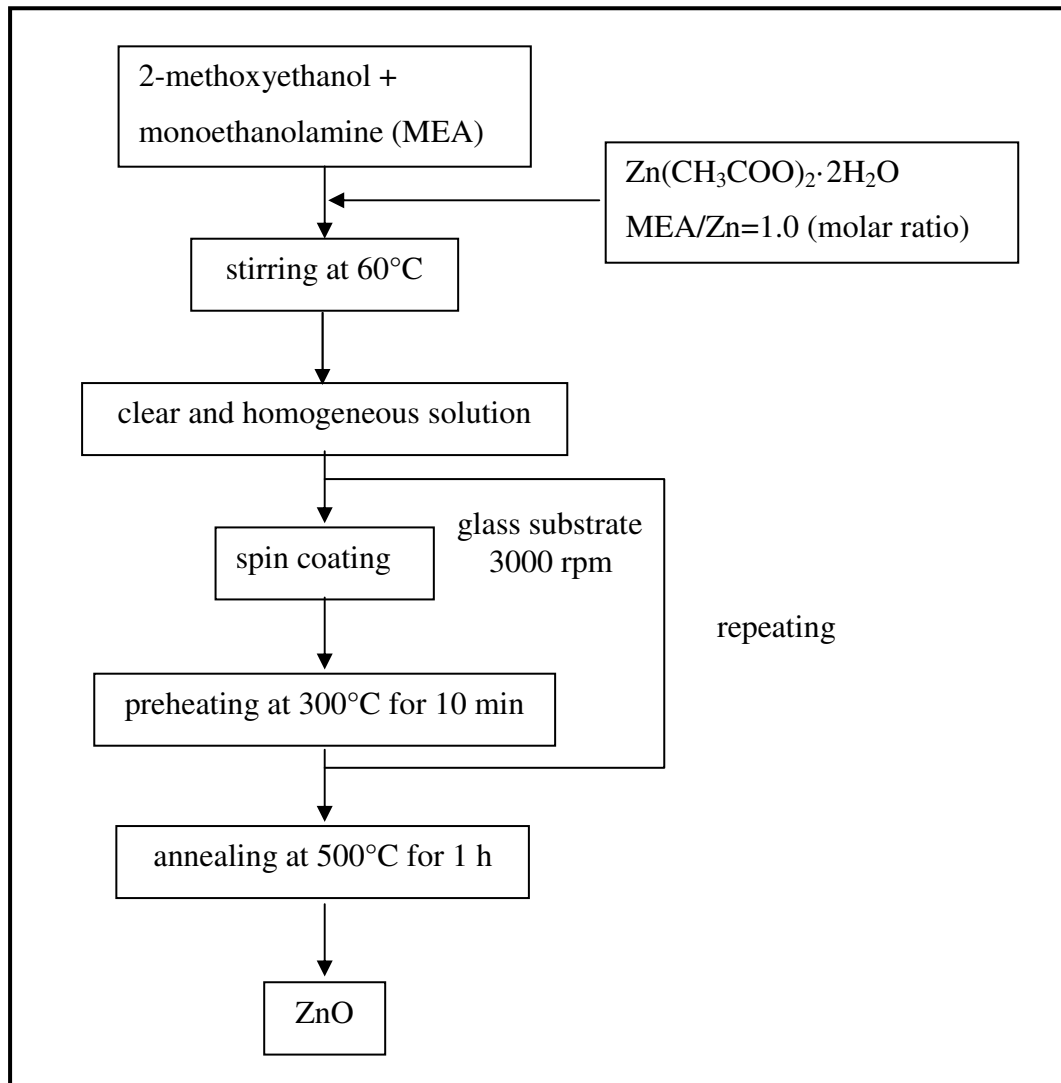
Figure 7. The flow chart showing the procedure for preparing the nanostructured ZnO thin film.

Source: Caglar *et al.,* (2009)

In their study, 2-methoxyethanol and monoethanolamine (MEA) were used as a solvent and stabilizer, respectively. The average grain size of the prepared ZnO thin film was found to be 28 nm. This film has a high transparency with the average

transmittance higher than 90% in visible region. The dependence of electrical conductivity of the film on temperature was measured so as to identify the dominant conductivity mechanism. From this study, they found that the conductivity mechanism of the film is the thermally activated band conduction. Moreover, the electrical conductivity and optical results revealed that the ZnO film is an *n*-type nanostructured semiconductor with a direct band gap of about 3.30 eV at room temperature.

Jiwei *et al*., (2000) prepared the ZnO thin film on various substrates by sol-gel process. The sol was prepared in 2-propanol and it was stabilized by diethanolamine ($HN(CH_2CH_2OH)_2$, DEA). The molar ratio of DEA to zinc precursor was kept constant at 1:1. The films were coated at a spinning speed of 2500 rmp for 30 s. These thin films exhibited a strong orientation along *c*-axis and their grain size was increased with increasing of heat treatment temperature. The optical propagation loosed was however increased because of the scattering at the interface of ZnO/SiO_2, and the ZnO grain. Dielectric constant and resistivity of thin films deposited on $Pt/SiO_2/Si(111)$ substrates were in the range of 7-13 and 1.7×10^4 to 9.8×10^5 Ω.cm, respectively.

Dutta *et al*., (2008) prepared ZnO thin flims on glass substrates by sol-gel drain coating technique at various concentrations of the sol. $Zn(CH_3COO)_2 \cdot 2H_2O$ was used as a starting material. DEA and isopropyl alcohol were used as stabilizer and solvent, respectively. After the substrates were heated at 550°C for 1 h in air, the randomly oriented ZnO phase was found in XRD pattern. The higher sol concentration resulted in the increase in grain size. The studies on the optical properties showed that the band gap value increased from 3.27 to 3.30 eV when the sol concentration was increased from 0.03 to 0.1 M.

Mandal *et al*., (2008) investigated the dependence of photoluminescence characteristics on temperature of nanocrystalline ZnO thin films deposited on p-Si(100) substates. Sol was prepared by mixing of zinc acetate dihydrate and DEA in 2-propanol. The molar ratio of Zn^{2+}: DEA was 1:2. After coating process, the films were annealed at 600°C in oxygen atmosphere. From the results, the as-deposited films showed amorphous phase whereas the annealed films performed crystalline phase. The green emission gradually decreased with an increase

of temperature between 450-750°C and the minimum emission occurred when the films were annealed at 600°C because of the minimum defect state emission.

Chen *et al*., (2009) prepared ZnO thin films on the quartz substrate by sol-gel method. To prepare the sol solution, zinc acetate dihydrate was mixed with a DEA in hydrate methanol, and the molar ratio of DEA to zinc acetate was 1. The spin coating method with a rotation rate of 3000 rpm was used to coat for all samples. The films were annealed at different temperatures for 1 h under O_2 atmosphere. All ZnO thin films corresponded to the wurzite-type ZnO structure and preferred orientation along (002) plane. With increasing the annealing temperature, the intensity of the (002) diffraction peak increased. The prepared ZnO thin film also showed a strong UV emission band at 381 nm and a very weak green emission band at 510 nm.

Vafaee and Ghamsari (2006) prepared ZnO nanoparticles by a novel sol-gel route. The starting material used in this study was zinc acetate dihydrate and solvent was ethanol, as well as triethanolamine (TEA) was used as stabilizer. The best ratio of each component was selected based on ZnO that gave better optical properties. The molar ratio of TEA to zinc acetate was 3:5. Experimental results showed that the prepared ZnO nanoparticles by this method had high intensity of photoluminescence.

Xie *et al*., (2006) reported that submicrometer-sized ZnO particles with well-defined ellipsoidal morphologies were obtained by sonication at temperature below 80°C in aquesous solution. ZnO particles were synthesized by hydrolysis of zinc acetate dihydrate in the presence of different TEA concentrations. The morphology of ZnO particles can be systematically changed from elongated rugby ball-like ellipsoidal to half-ellipsoidal by increasing of TEA concentration. TEA may serve as a surface modifier, presumably bound to Zn^{2+}. Owing to the absorption of TEA which acted as a capping agent, ions may bound to the Zn^{2+} (0001) surfaces. The surface interaction can inhibit the ZnO crystals elongated perpendicular to (0001) planes, thus the morphology of ellipsoidal particles was changed to half-ellipsoidal. The spatial resolved CL measurements showed that the UV luminescence was remarkably strong at the base of the bigger side of the ellipsoidal particles, and the

UV luminescence spectra were of either a wide stripe or a narrow stripe at the core of the ellipsoidal particles depending on the growth temperature.

Fu *et al*., (2008) investigated a single-crystal ZnO flocky sphere formation. This shape was prepared from a reaction between zinc nitrate and TEA in isopropyl alcohol at 80°C for 1 h. The flocky sphere shape was suggested by the aggregation of nanoparticles. In the first stage, the surfaces of ZnO particles were believed being covered with TEA ligands. Subsequently, the uniformly distributed primary particles aggregated together, giving rise to a formation of a flocky sphere as shown in figure 8.
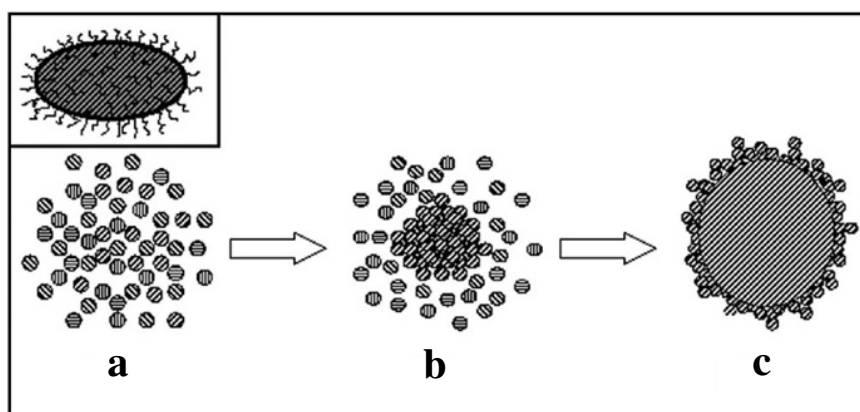
Figure 8. The process of three-dimension-oriented attachment.

Source: Fu *et al*., (2008)

Xu *et al*., (2008) presented a novel one-step method to synthesize nano/micro-sized ZnO sphere. In a typical procedure, zinc nitrate hexahydrate was mixed with TEA and then the mixed solution was transferred into a Teflon-lined autoclave. This solution was heated at 160°C for 2 h. The obtained powders showed the XRD pattern of a typical ZnO structure. The particle diameter of powders was increased with decreasing of the volume ratio of TEA to H_2O. The aggregation of nanoparticles to form spherical ZnO particles can be explained by a novel mechanism called oriented aggregation as shown in figure 9.
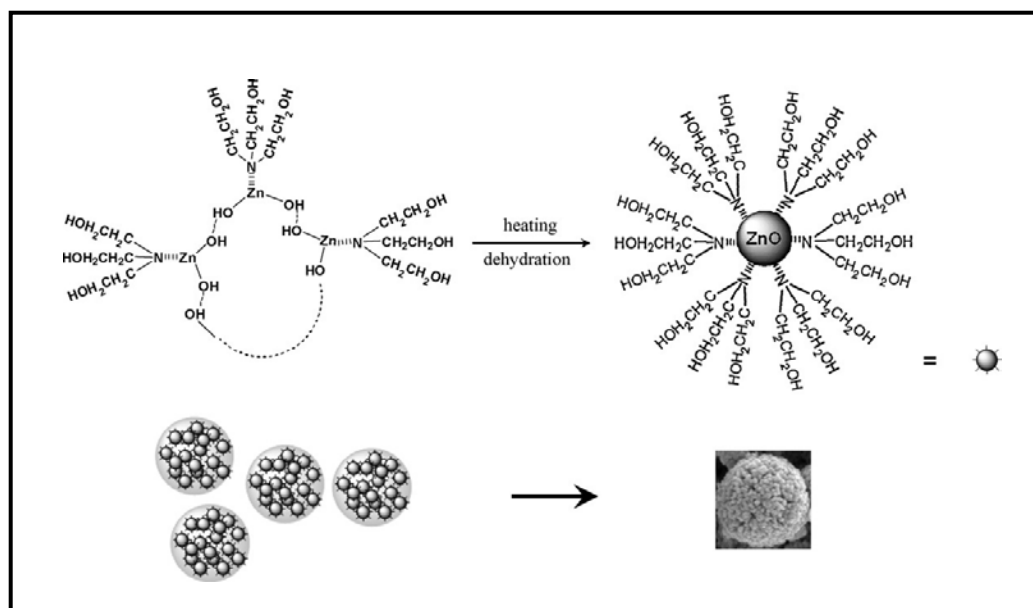
Figure 9. Schematic illustration of the formation mechanism of the as-obtained ZnO nano/micro-sphere.

Source: Xu *et al*., (2008)

Tang *et al*., (2009) prepared ZnO particles by hydrolysis of $ZnSO_4$ in the presence of TEA at different ratios of TEA/Zn^{2+}. After addition of NaOH solution with different molar ratios of NaOH/Zn^{2+}, the white precipitates were obtained. In this synthesis, TEA acted as a complexing agent and NaOH contributed to transformation of zinc precursor into ZnO particles. They proposed a possible mechanism that could be described as follows, TEA could react with Zn^{2+} ions to get positive complexes and influence the amount of negative $Zn(OH)_4^{2-}$ ions. The positive complexes could adsorb on the negative (00-1) plane and the negative $Zn(OH)_4^{2-}$ ion could adsorb on the (001) plane by electrostatic force, resulting in the crystal growth along these two planes. At molar ratio of TEA/Zn^{2+} = 1, the growth along (001) and (00-1) could be occurred. But if the molar ratio of TEA/Zn^{2+} was increased to 3, the growth along (00-1) plane would be induced because of the coordination of TEA and NaOH.

Kajbafvala *et al*., (2009) reported the rapid synthesis of nanostructure sword-like ZnO wires through a microwave-assisted route. In the synthetic procedure, zinc acetate dihydrate was added to the solution of TEA and methanol. After that solid NaOH pellet was slowly added into the above solution until pH of solution

reached to 9.5. After the solution was cooled to room temperature, the white precipitates were separated by centrifugation. The product showed the diffraction peaks in accordance with wurtzite ZnO structure. The SEM images clearly revealed that the aspect ratio of ZnO wires with sword-like tips was estimated being in the range of 20-25. The sword-like ZnO nanowires had high crystallinity with an average crystallite size of about 53 nm and they showed a UV emission and a visible green band in the PL spectrum.

Zeng *et al*., (2009) reported the preparation of the nut-like ZnO microcrystals via a simple hydrothermal route. Zinc acetate dihydrate and TEA were mixed together. After ammonia was slowly added dropwise into solution until the pH of solution was 9.5, the white precipitates were formed and they were then transferred into a Teflon-lined stainless steel autoclave for the hydrothermal treatment at 95°C for 2 h. The XRD pattern of the as-prepared powders demonstrated that all of the diffraction peaks were indexed as ZnO wurtzite structure. The ZnO shaped a nut-like structure with an average diameter of about 1.8 µm and 2.2 µm in length. It exhibited well-resolved hexagonal edges and corners, as well as the ZnO (001) plane is covered with aggregated nanoparticles.

The photocatalysis is the acceleration of a photoreaction in the presence of a catalyst. Although most of the photocatlytic studies use either synthetic or commercial TiO_2, recently some studies have been carried out to evaluate the priority of other metal oxides. Among the other semiconducting oxides, ZnO appears to be a highly promising photocatalyst. The photocatalytic degradation of dye in a waste from dyeing process is one of the applications of ZnO as a photocatalyst. Upon irradiation, valence band electrons are promoted to the conduction band leaving a hole behind (Behnajady *et al*., 2006; Sobana *et al*., 2007):

$$ZnO + h\nu \longrightarrow ZnO (e_{CB}^- + h_{VB}^+)$$

These generated species can either recombine and dissipate the energy as heat or react with oxygen or water molecules to produce strong oxidizing hydroxyl radicals:

$$e_{CB}^- + O_2 \longrightarrow O_2^{\bullet-}$$

$$h_{VB}{}^{+} + H_2O \longrightarrow H^{+} + OH^{\bullet}$$
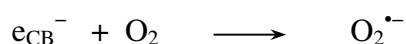
The hydroxyl radical is a powerful oxidizing agent and attacks to organic compounds and intermediates are formed. These intermediates react with hydroxyl radicals to produce final products:

$$OH^{\bullet} + dye \longrightarrow H_2O + Dye\ intermediate$$

$$Dye\ intermediate + OH^{\bullet} \longrightarrow CO_2 + H_2O + mineralization\ products$$

Chakrabarti *et al*., (2004) reported that high effective in removal of Methylene Blue and Eosin Y with ZnO from aqueous solution. In addition to the removal of colors, the reaction simultaneously reduced the COD (chemical oxygen demand), suggesting that the dissolved orgnics were at least partially oxidized.

Lu *et al*., (2007) synthesized the ZnO nanotubes by thermal oxidation of Zn nanowire. They investigated their photoctalytic activity versus ZnO particle by employing the photocatalytic degradation of Methyl Orange (MO) at ambient temperature. Using their ZnO nanotubes, the concentration of MO reduce to 0 % when the irradiation time is prolonged to 40 min, whereas the ZnO particles require at least 90 min to decolorize the MO completely. An enhanced photocatalytic activity of prepared ZnO nanotube due to high surface-to-volume ratio and abundant oxygen vacancies near the surface of ZnO nanotube.

Sobana *et al*., (2007) investigated the photocatalytic degradation of an azo dye acid red 18 (AR18) using various semiconductors as a photocatalyst in aqueous solution UV irradiation. ZnO showed as the most active catalyst that exhibited a higher activity than TiO_2. The addition of oxidants $(NH_4)_2S_2O_8$ and $KBrO_3$ enhances the dye removal process. On the contrary, the addition of H_2O_2 decreases the photocatalytic degradation.

Wang *et al*., (2007) showed that the photocatalytic activity of ZnO depends on a preparation method rather than particle sizes and morphology. Using Methyl Orange solution, ZnO with diameter of 50 nm prepared by thermal

evaporation method showed the highest photocatalystic activity. Furthermore, the tetrapod ZnO powders had the higher efficiency than irregular ZnO particles. However, the smallest (10 nm) ZnO particles prepared by chemical deposition method indicated the lower efficiency contrast to ZnO powders with 200 nm in size prepared by thermal evaporation method.

5. Objectives

5.1 To prepare the modified-ZnO particles with aminoalcohol (MEA, DEA and TEA) by precipitation method.

5.2 To study the difference in morphology and optical properties of aminoalcohol modified-ZnO particles.

CHAPTER 2

INSTRUMENTATION

1. X-ray Powder Diffraction

X-ray diffraction (XRD) is a non-destructive technique primarily used for phase identification of a crystalline material and this technique provides information on unit cell dimensions. Most of all solid materials can be described as crystalline and when X-ray interacts with a crystalline phase, a diffraction pattern is generated as a result of the interaction between the incident X-ray and the atomic architecture of the solid.

1.1 Fundamental principles of XRD

X-rays are electromagnetic radiation with typical photon energies in the range of 10-100 eV or wavelength between roughly 0.01 nm and 10 nm. This wavelength lies between ultraviolet light and gamma rays in the electromagnetic spectrum. For diffraction applications, only relatively short wavelengths X-ray in a range of a few angstroms to 0.1 angstrom are used. Because the wavelength of X-ray is comparable to the size of atoms, they are ideally suited for probing the structural arrangement of atoms and molecules in a wide range of materials. The energetic X-rays can penetrate deeply into the materials and provide information about the structure, such as crystallite size and lattice parameter.
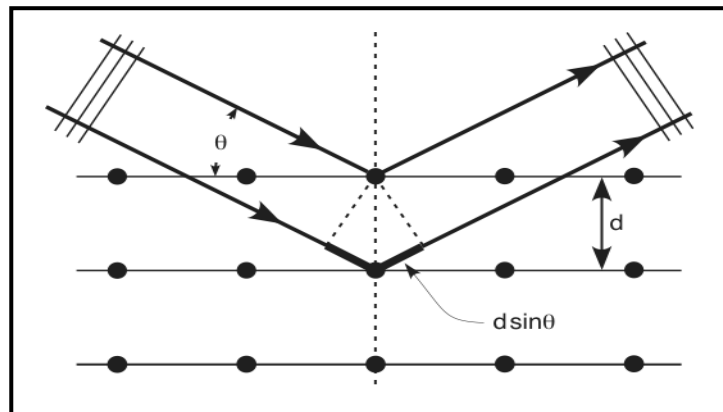
Figure 10. Bragg diffraction condition.

Source: http://upload.wikimedia.org/wikipedia/commons/0/0a/Bragg_diffraction.png

If an incident X-ray beam encounters a crystal lattice, general scattering occurs as seen in figure 10. Although most scattering interferes with itself and is eliminated (destructive interference), diffraction occurs when scattering in a certain direction is in phase with scattered rays from other atomic planes. Under this condition, the reflections combine to form new enhanced wave fronts that mutually reinforce each other (constructive interference). In 1912, W.L. Bragg recognized a predictable relationship among several factors. The relation by which diffraction occurs is known as the Bragg law or Bragg equation, and it can be expressed below:

$$2d \sin\theta = n\lambda$$

where n is a small integer giving the order of diffraction analogous to a ruled grating, (an integer), λ is a wavelength of the characteristic line X-rays from the X-ray tube and usually the CuK_α doublet with $CuK_{\alpha 1} = 0.1540562$ nm, d is a distance (nm) between a set of parallel lattice planes, and θ is a angle between the incident collimated X-ray beam and an atomic lattice plane in the crystal.

Each crystalline solid has unique atomic architecture and it consequently has a unique characteristic X-ray powder pattern. These patterns can be used as "fingerprints" for identification of solid phases.

This Bragg law relates the wavelength of electromagnetic radiation to the diffraction angle and the lattice spacing in a crystalline sample. These diffracted X-rays are then detected, processed and counted. By scanning the sample through a range of 2θ angles, all possible diffraction directions of the lattice should be attained due to the random orientation of the powdered material. Conversion of the diffraction peaks to d-spacings allows the identification of the mineral because each mineral has a set of unique d-spacings. Typically, this is achieved by comparison of d-spacings with standard reference patterns.

The X-ray diffraction pattern of a pure substance is, therefore, like a fingerprint of the substance. The powder diffraction method is thus ideally suited for characterization and identification of polycrystalline phases (Scintag Inc., 1999).
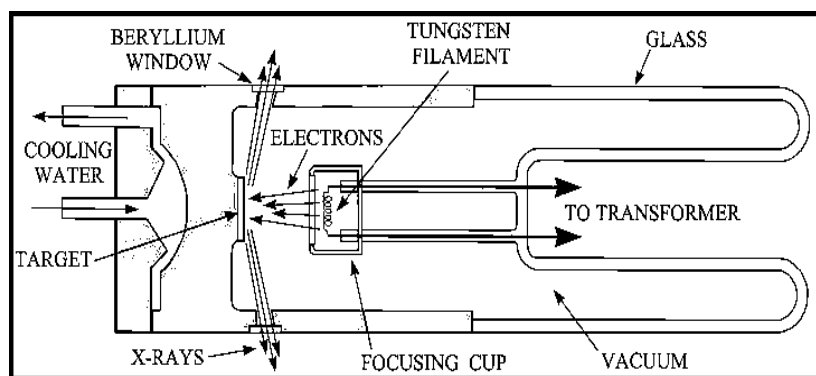
Figure 11. Schematic cross section of an X-ray tube.
Source: http://pubs.usgs.gov/of/2001/of01-041/htmldocs/images/xrdtube.jpg

X-ray diffractometers consist of three basic elements: an X-ray tube, a sample holder, and an X-ray detector. X-rays are generated in a cathode ray tube by heating a filament (cathode) to produce electrons, accelerating the electrons toward a target by applying a voltage (normally in order of 30 KV to 50 KV), and bombarding the target material (anode) with electrons (Figure 11). When electrons have sufficient energy to dislodge inner shell electrons of the target material, characteristic X-ray spectra are produced (Figure 12a). These spectra consist of several components, the most common being K_α and K_β (Figure 12b).
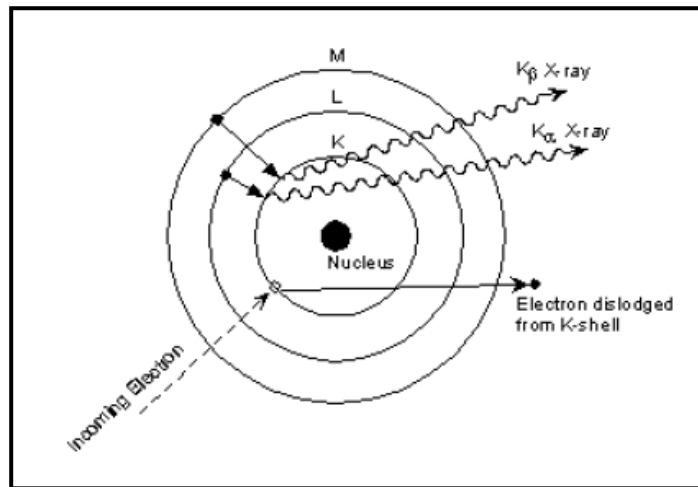
(a)

Source: (Connolly, 2007) www.unm.edu/xrd/xrdclass/03-GenX-rays.pdf
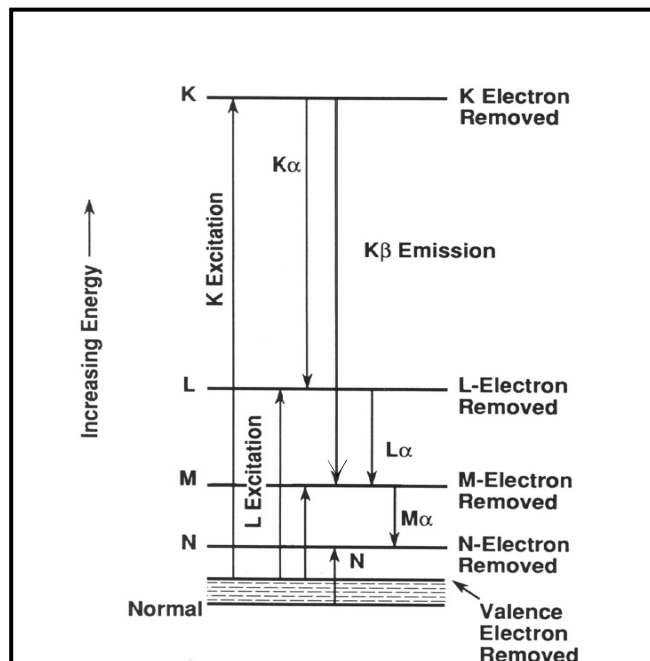
(b)

Source: www.mtsc.unt.edu/FACULTY/bgorman/3020/3020%20Lecture%208%20-%20XRD.pdf
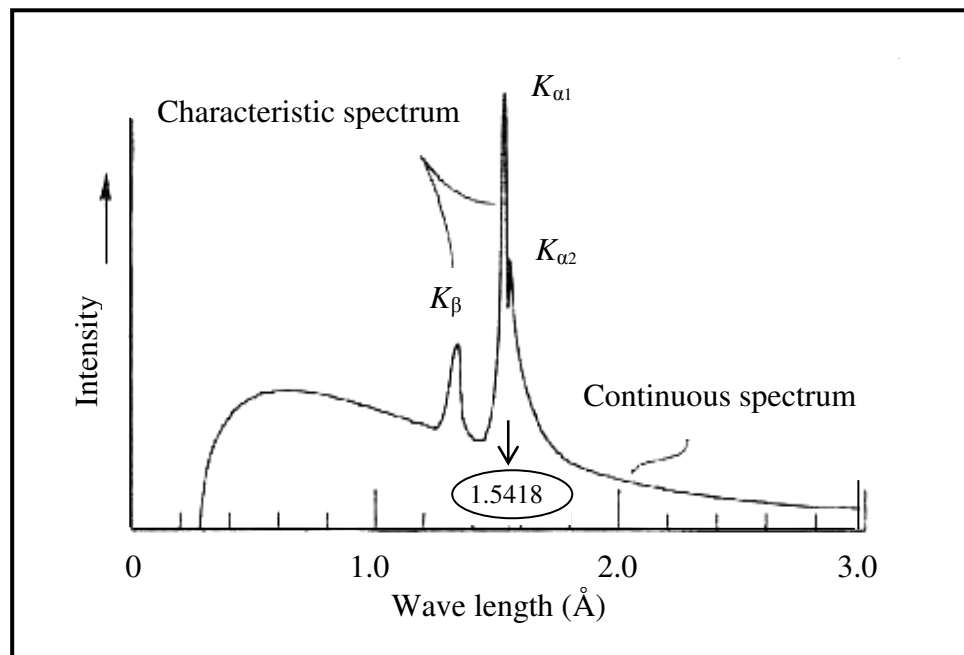
Source: www.mtsc.unt.edu/FACULTY/bgorman/3020/3020%20Lecture%208%20-
%20XRD.pdf

(c)

Figure 12. (a) shows schematically in the diagram. An incoming electron displaces a
K-shell electron. If an L-shell electron moves to replace it, a K_α X-ray is
produced. If an M-shell electron moves to replace it, a K_β X-ray is
produced. (b) shows energy-level diagram for an atom illustrating the
excitation of the K, L, M and N shells and the formation of K_α, K_β, L_α and
M_α X-rays, and (c) shows that an X-ray spectrum consist of two different
radiation continuous and characteristic radiation for copper.

K_α consists, in part, of $K_{\alpha 1}$ and $K_{\alpha 2}$. $K_{\alpha 1}$ has a slightly shorter
wavelength and twice the intensity as $K_{\alpha 2}$ (Figure 12c). Copper is the most common
target material for single-crystal diffraction, with Cu K_α radiation = 1.5418 Å.
Filtering, by foils or crystal monochrometers, is required to produce monochromatic
X-rays needed for diffraction. $K_{\alpha 1}$ and $K_{\alpha 2}$ are sufficiently close in wavelength such
that a weighted average of the two is used.

After producing from X-ray tube, X-rays are collimated and directed onto the sample. As the sample and detector are rotated, the intensity of the reflected X-rays is recorded. When the geometry of the incident X-rays impinging the sample satisfies the Bragg equation, constructive interference occurs and a peak intensity occurs. A detector records and processes this X-ray signal and converts the signal to a count rate which is then output to a device such as a printer or computer monitor.

The geometry of an X-ray diffractometer is such that the sample rotates in the path of the collimated X-ray beam at an angle θ while the X-ray detector is mounted on an arm to collect the diffracted X-rays and rotates at an angle of 2θ. The instrument used to maintain the angle and rotate the sample is termed a goniometer. This arrangement is called the Bragg-Brentano parafocusing geometry (Figure 13) and data is collected at 2θ.
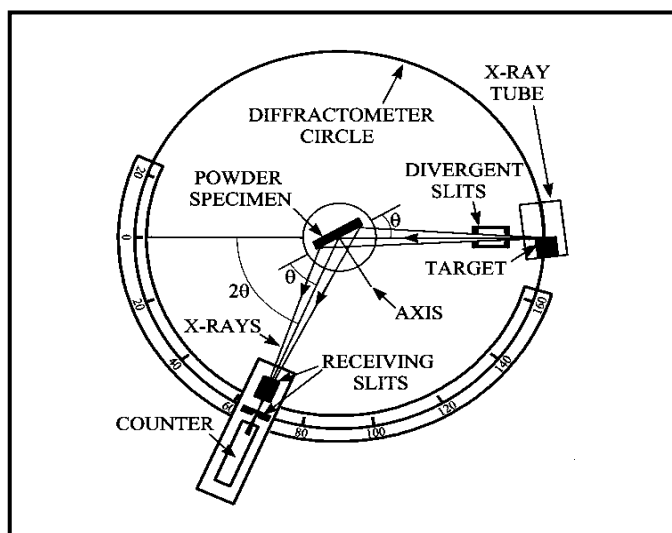
Figure 13. Geometric arrangement of the Bragg Brentano diffractometer.
Source: http://pubs.usgs.gov/of/2001/of01-041/htmldocs/images/xrdschem.jpg

From the wurtzite structure, the interplanar distance of {*hkl*} plane is related to the lattice parameters *a* and *c* via the Miller indices *hkl*:

$$\left[\frac{1}{d_{hkl}}\right]^2 = \frac{4}{3}\left[\frac{h^2 + k^2 + hk}{a^2}\right] + \frac{l^2}{c^2}$$

It is well-known that the XRD technique provides the information on lattice parameter. If Miller indices can be assigned to the various reflections in the powder pattern, it becomes possible to determine the cell constant. These are directly related to 2θ and *h, k, l* through the relationships derived from the combination of Bragg's law and *d*-spacing expession and summarized in the table 1.

Table 1. Expression for *d*-spacing in the different crystal systems

Crystal System	Expression for d_{hkl} terms of lattice parameters and Miller indices
Cubic	$\dfrac{1}{d^2} = \dfrac{h^2 + k^2 + l^2}{a^2}$
Tetragonal	$\dfrac{1}{d^2} = \dfrac{h^2 + k^2}{a^2} + \dfrac{l^2}{c^2}$
Orthorhombic	$\dfrac{1}{d^2} = \dfrac{h^2}{a^2} + \dfrac{k^2}{c^2} + \dfrac{l^2}{d^2}$
Hexagonal	$\dfrac{1}{d^2} = \dfrac{4}{3}\left[\dfrac{h^2 + k^2 + hk}{a^2}\right] + \dfrac{l^2}{c^2}$
Monoclinic	$\dfrac{1}{d^2} = \dfrac{1}{\sin^2\beta}\left[\dfrac{h^2}{a^2} + \dfrac{k^2 \sin^2\beta}{b^2} + \dfrac{l^2}{c^2} - \dfrac{2hl\cos\beta}{ac}\right]$

Source: Hammond, (1990)

Crystallite size is one kind of effects that can change diffraction peak widths. As the crystallites in a powder get smaller, the diffraction peaks at a powder pattern get wider. The crystallite size is easily calculated as a function of peak width (specified as the full-width at half maximum peak intensity, FWHM) peak position and wavelength of X-ray. This is known as the Scherrer's formular:

$$D = \frac{0.9\lambda}{\beta \cos\theta}$$

where D is the average crystallite size, λ is the wavelength of incident X-ray, θ is the Bragg angle of diffraction lines, β is the full-width half-maximum in radians

1.2 Sample preparation for XRD

XRD samples should be well-ground in a mortar and pestle or a ball mill. This creates a uniform particle size and ensures that all possible crystallite orientations are present in the sample. The well-fine sample is then mounted into the samples holder. Sample's requirement for powder XRD depends on the nature of the material. A typical sample holder makes of an aluminum plate with a circle hole in the center. Normally, the sample holder is a 20 mm of diameter and a 2 mm thick. It can be modified when the sample quantity is a problem. For materials that diffract strongly (many inorganic materials), a few milligrams of the sample is then spread on the tape and smoothed flat. The tape is primarily amorphous and so does not generally interfere with the pattern being collected.

2. Scanning Electron Microscope

A scanning electron microscope (SEM) is basically type of electron microscope that three-dimensional-like image of the specimen surface is formed. The electrons interact with the atoms that make up the sample producing signals that contain information about the sample's surface, topography, microstructure and particle size distribution.

2.1 Fundamental principles of SEM

In SEM, primary electrons are emitted by thermonically or field emission from a cathode filament (W or LaB_6) or a field emission gun (W-tip) and after that accelerated with high energy typically 1-30 KV. The electron beam must be demagnified by electron lenses and places a much smaller focused electron spot on the specimen. Two pairs of electronmagnetic deflection coils (scan coils) are used to sweep the beam across the specimen (Figure 14). The magnification (M) of the image is the ratio of length of the raster on the viewing screen to the corresponding length of rester on the specimen.
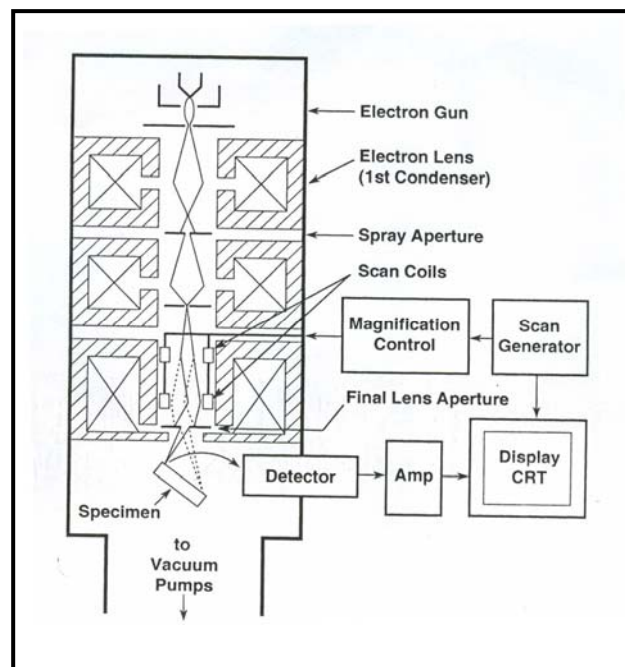
Figure 14. Schematic for a generic SEM.

Source: Goldstein *et al*., (2003)

The types of signals produced when the electron beam enters the specimen, include secondary electrons (SE), back scattered electrons (BSE), characteristic X-rays, (cathodoluminescence), specimen current and transmitted electrons as shown in figure 15. Each signal requires specialized detector for its detection that is not usually all present on a single machine. Backscattered and secondary electrons, the principal signals used to form image in SEM, are generated within the interaction volume.
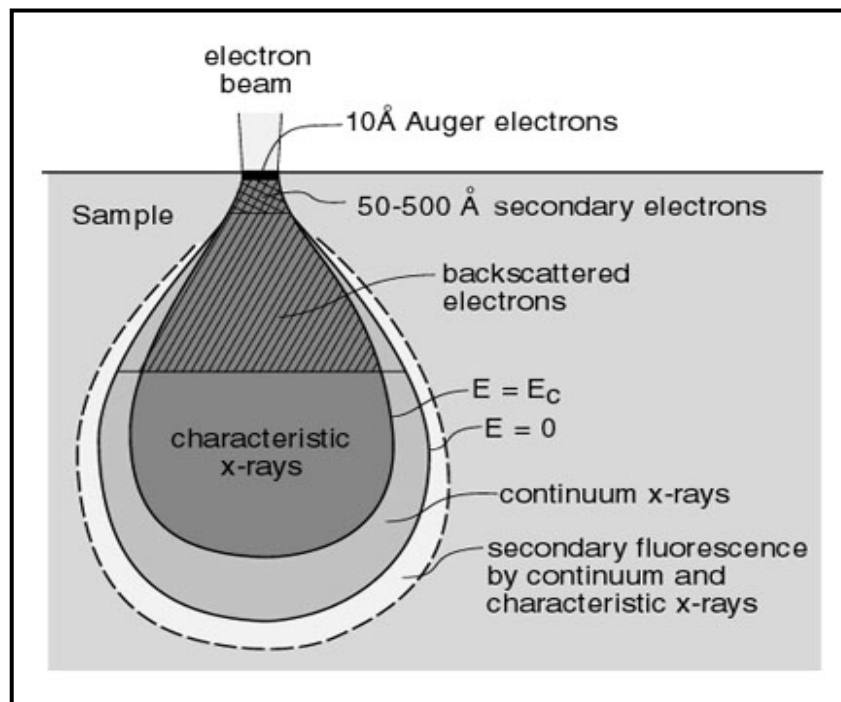
Figure 15. Generalized illustration of interaction volumes for various electron-
        specimen interactions.

Source: www4.nau.edu/.../Microprobe-SEM/Signals.html

Secondary electrons (SE) are loosely bound outer shell electrons from the specimen atoms which receive sufficient kinetic energy during inelastic scattering of electrons to be ejected from the atom and set into motion. They are used for surface topographic (shape, size, surface texture) studies. The secondary electron coefficient varies with the specimen tilt angle so this effect introduces a number component to topographic contrast in the secondary electron signal.

Backscattered electrons (BSE) consist of high-energy electrons originating in the electron beam, that are reflected or back-scattered out of the specimen interaction volume by elastic scattering interactions with specimen atoms. Since heavy elements (high atomic number) backscatter electrons more strongly than light elements (low atomic number), and thus appear brighter in the image, BSEs are used to detect a contrast between areas with different chemical compositions. (http://en.wikipedia.org/wiki/Scanning_electron_microscope-10/11/2008).

2.2 Sample preparation for SEM

Even with a conducting specimen such as a metal, the remaining beam current must flow from the specimen to ground to avoid the accumulation of charge in the junction. It must be noted that if the path from the specimen surface to ground is broken (non-conductive sample), the electron injected into the specimen by the beam will accumulate, and the specimen will develop a high negative electrical charge relative to ground. In fact, the high resistivities of insulators prevent the smooth motion of the electron injected by the beam through the specimen to ground, so that the electrons accumulate in the immediate vicinity of the beam impact, raising the local potential. The resulting diverse set of phenomena is referred to as "charging" and leads to strong effects in SEM images.

The best and simplest way to overcome the charging problems is to deposit a thin metal layer on the surface of the sample. Sputter coating is a popular and relatively simple way of applying a coating layer of metals and their alloys to nonconductive substrates. The target material is exposed to an energized gas plasma formed from a heavy inert gas such as argon. The target surface is eroded by the plasma and atoms are ejected and collide with residual gas molecules. Target atoms have a short mean free path and provide multidirectional coating on a stationary specimen.

3. UV-Vis spectroscopy

Ultraviolet-visible (UV-Vis) spectroscopy uses light in the visible and near ultraviolet ranges to excite the outer electrons. At these wavelengths, molecules undergo electronic transitions. When visible or ultraviolet light is absorbed by the valence electrons of the material, these electrons are promoted from their ground states to higher energy excited states (Figure 16). The difference between the initial and final intensities is recorded. When plotted into a spectrum as wavelength against absorbance (A), the absorbance is defined by using the Beer-Lambert law as follow:

$$A = -\log (I/I_0)$$

where A is the measured absorbance, I_0 is the intensity of incident light at a given wavelength, and I is the transmitted intensity, respectively. Most spectrometers display absorbance on the vertical axis, and the commonly observed range is from 0 (100% transmittance) to 2 (1% transmittance). The wavelength of maximum absorbance is a characteristic value designated as λ_{max}.
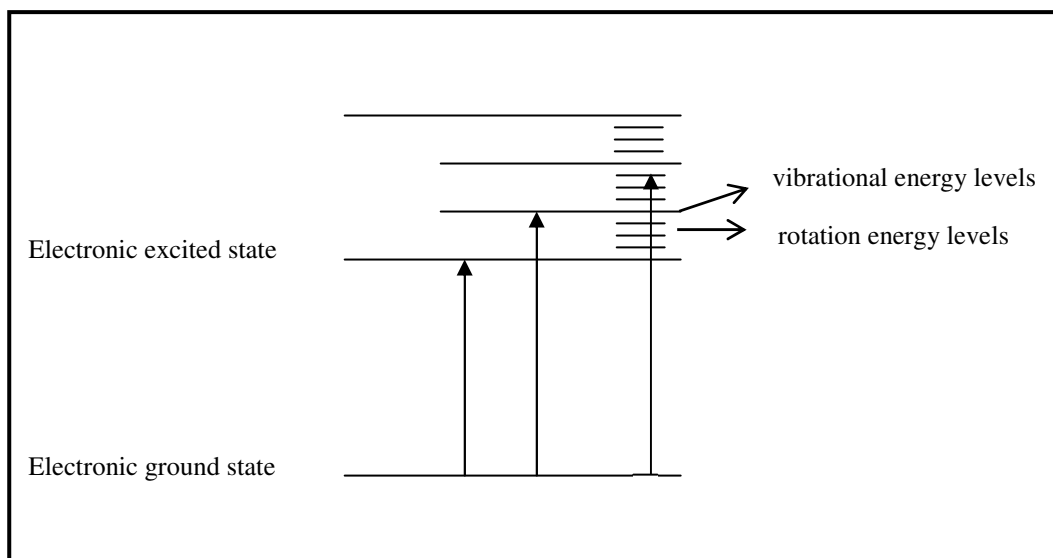
Figure 16. Illustration of the electronic transitions process during light absorption.

In a crystal, the band gap is defined as the minimum energy between the occupied valence band and empty conduction band. The Tauc gap is found by extrapolating the linear part of a plot of $(\alpha E)^{1/2}$ against the photon energy. The intercept of this line with photon energy axis gives the value of the Tauc optical gap.

4. Photoluminescence

Luminescence is the emission of photon (in ultraviolet, visible or infrared region) from an electronically excited species. The various types of luminescence are classified to the mode of excitation (Valeur, 2002). Photoluminescence (PL) is a process in which a chemical compound absorbs the photon (electromagnetic radiation), thus jumping to a higher electronic energy state, and then radiates photons, returning to a lower energy states. Photo-excitation causes

electrons within the material to move into permissible excited states. When these electrons return to their equilibrium states, the excess energy is released and may include the emission of light, or luminescence.

Photoluminescence is a non-destructive and a powerful technique used for characterization, investigation and detection of defects or for measuring the band-gaps of materials. In semiconductor, PL involves the irradiation of the sample to be characterized with photon energy greater than band-gap energy of that material. Free electrons are created in the conduction band together with the free holes in valance band. When these carriers will energetically relax down the band edge, it may do so through radiative (release of a photon) or non-radiative (no photon production) recombination. The detected luminescence signals could result from the band-to-band recombination, intrinsic crystalline defects, dopant impurities, or other extrinsic defect levels by several radiative transitions between the conduction band and valence band, exciton, donor and acceptor levels, as shown in figure 17.

Figure 17. Schematic illustration of common recombination process. (The conduction band, E_{CB}, occupied by free electrons, and the valance band, E_{VB}, occupied by free holes, are represent in addition to donor, E_D, and acceptor, E_A trapping centers within the forbidden gap).

The first described transition is radiative band-to-band or direct recombination (Figure 17(a)), which dominate at room temperature and can be used to estimate the band gap energy (E_g) of materials. The band-to-band tra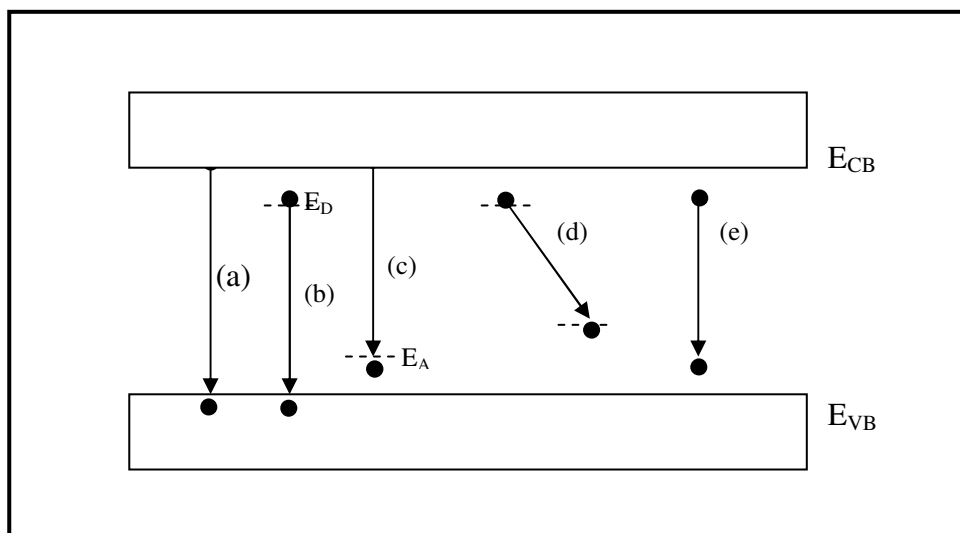nsition contains the recombination of free electrons and free holes. This transition occurs when an electron falls from its conduction band state into the empty valence band state associated with the hole. For indirect semiconductors, a band-to-band recombination process is unlikely because the electrons at the bottom of the conduction band have a non zero crystal momentum with respect to the holes at the top of the valence band.

Such transition involving the electrons trapped on the donors and holes, are known as bound-exciton (Figure 17(b)). An electron bound to a donor can recombine directly with a free hole from a valence band. This kind of recombination is called free-to-bound (FB) transition (Figure 17(c)).

When both donor and acceptor impurities are present in semiconductors, coulombic interaction between a hole bound to an acceptor recombines with an electron bound to a donor in donor-acceptor pair (DAP) transition (Figure 17(d)). Both the donor and the acceptor are neutral before the recombination (i.e. the dornor positively and the acceptor negatively charged).

Excitonic recombination can occur following the generation of an electron-hole pair. Coulombic attraction lends to the formation of an excited state in which an electron and the hole remain bound to each other in a hydrogen-like state, refered to as a free exciton (Figure 17(e)).

The basic components of a photoluminescence spectrometer are shown schematically in figure 18. The excitation source is a special xenon flash tube, which produces an intense, short duration pulse of radiation over the spectral range of the instrument. Energy from the source is focused by the ellipsoidal mirror and reflected by the toroidal mirror onto the entrance slit of the excitation monochromator. A narrow wavelength band emerges from the exit slit, with the center wavelength being determined by the setting of the grating, the angle of which is controlled by a stepper motor. The majority of the excitation beam is transmitted to the sample via the focusing toroidal mirror, a small proportion is reflected by the beam splitter onto the referent photodiode. Energy emitted by the sample is focused by the toroidal mirror onto the entrance slit of the emission monochromator and go to detector.
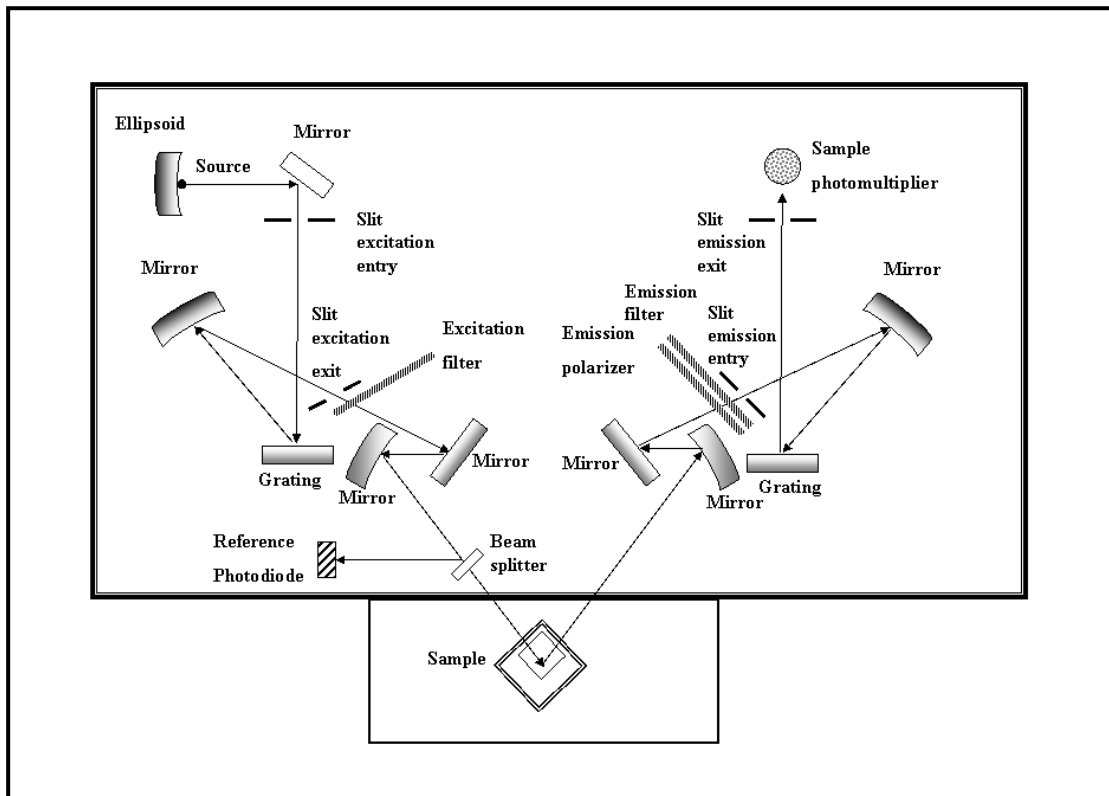
Figure 18. The optical layout.

Source: Perkin Elmer Inc., (2000)

CHAPTER 3

EXPERIMENTAL

1. Chemicals and Reagents

Chemicals and reagents used in this work were purchased from various suppliers as shown in table 2 and they were used as received.

Table 2. List of chemicals and reagents.

Chemicals and reagents	Suppliers
Zinc nitrate hexahydrate, AR grade	Fluka, Japan
Monoethanolamine, AR grade	Fluka, Japan
Diethanolamine, AR grade	Sigma-Aldrich, USA
Triethanolamine, AR grade	Carlo Erba, Italy
Ammonia solution 30%, AR grade	Carlo Erba, Italy

2. Instruments

2.1. X-ray diffractometer (XRD)

X-ray diffraction patterns were carried out by the Philips X'Pert MPD diffractometer.

2.2. Scanning electron microscope (SEM)

The shape and size of all samples were measured using a JEOL, JSM-5800 LV scanning electron microscope.

2.3. Ultraviolet-visible (UV-Vis) spectrophotometer

Absorption spectra of ZnO powders were measured from a Shimadzu, UV- 2450 spectrophotometer.

2.4. Luminescence spectrometer (PL)

Room temperature luminescence of ZnO powders was investigated by a Perkin Elmer, LS 55 luminescence spectrometer.

2.5. Other equipments and apparatus

2.5.1. Analytical balance

A Mettler Toledo, AB204.S balance with significant of $\pm$ 0.0001 g was used to weigh chemicals all experiment.

2.5.2. Oven

A Memmert oven was used to dry the sample at 100°C for 1 h before calcination.

2.5.4. Furnace

A Carbolite RWF1300 furnace was used to eleminate the impurity phase from the sample in a suitable temperature for 1 h.

3. Procedure

Zinc oxide were synthesized by a precipitation method using an ammonia solution as precipitating agent. All experiments were prepared at a constant mole ratio of Zn^{2+}: NH_4OH = 1:2. Monoethanolamine (MEA), diethanolamine (DEA) and triethanolamine (TEA) were used as the capping agents.

3.1. Preparation of 0.20 M Zn^{2+} solution

Zn^{2+} solution was prepared by dissolving 17.8488 g of $Zn(NO_3)_2 \cdot 6H_2O$ in 150 mL of distilled water with continuous stirring until the clear solution was obtained.

3.2. Preparation of 0.40 M ammonia solution

16 mL of 30% ammonia solution was pipetted into 150 mL of distilled water. The mixture was stirred till homogeneous solution was obtained.

3.3. Synthesis of ZnO powder

150 mL of 0.20 M $Zn(NO_3)_2 \cdot 6H_2O$ solution was transferred into a round bottom flask. The capping agents (MEA, DEA and TEA) were pipetted into the Zn^{2+} solution separately with the constant mole ratios of Zn^{2+}: capping agents at 1:1, 1:2 and 1:3, respectivly. Then, the ammonia solution was added dropwise into the

capping agent-modified-Zn^{2+} solution under constant stirring at room temperature. These mixtures were continuously stirred at 70°C for 1 h to ensure that the complete reaction was occurred. After the precipitates were cooled to room temperature, they were filtered, rinsed with distilled water several times, then collected and dired at 100°C for 1 h in an oven and finally calcined at 500°C in air for 1 h.

3.4. Characterization

3.4.1. Phase identification and crystal structure

Phase formation and crystal structure were identified by XRD technique. The samples were ground and pressed in a sample holder. The XRD was operated in a normal mode without rotating the sample. The peak intensity was measured at interval of 0.02° over 2θ range of 28-72° using CuK_{α} radiation. The XRD operating parameters for all samples were shown in table 3.

Table 3. Operating parameters for XRD technique.

Parameters	Value
Step size	0.02°
Time per step	1 s
Divergence slit	0.5°
Anti-scattering slit	1°
Receiving slit	0.4 nm
Voltage	40 kV
Current	30 mA

3.4.2. Morphological study

Samples were mounted on a carbon tape which was glued on a brass stub. Because of lack in conductivity of ZnO powder, they were then coated with Au for 3 seconds by sputtering methode. A morphology of sample was examined by SEM using an accelerating voltage of 20 kV. Both shape and size of samples were investigated from the secondary electron micrograph at the suitable magnification.

3.4.3. Absorption spectra

Solid samples were ground and pressed in a sample holder. A diffuse reflected light from the sample relative to $BaSO_4$ as a white standard was corrected from 200-800 nm with $\Delta\lambda = 0.5$ nm using an integrating sphere method as shown in figure 19.
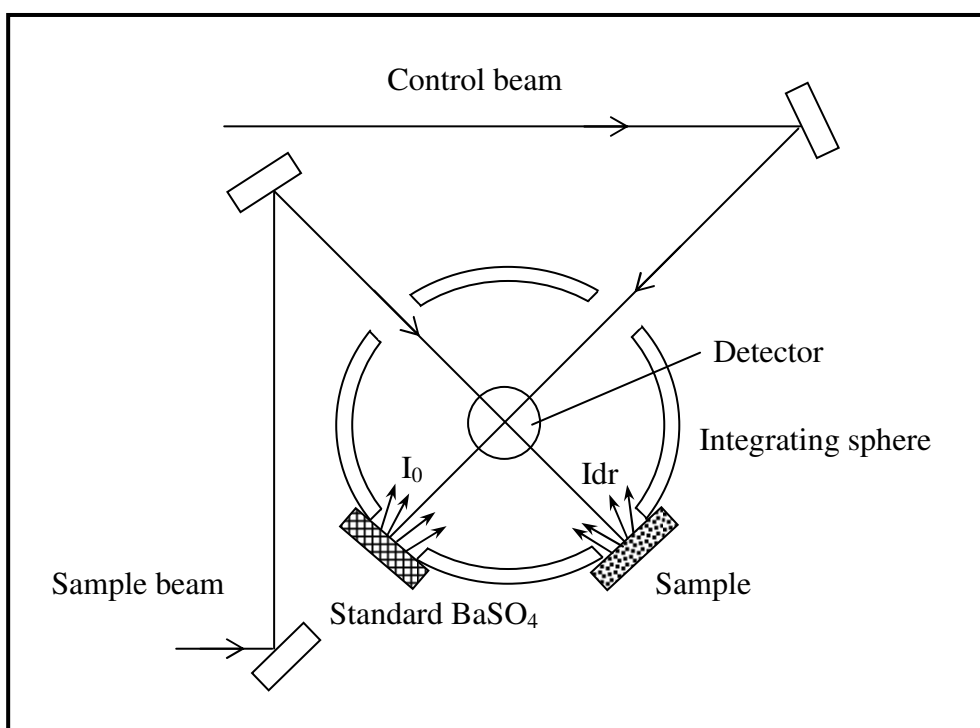
Figure 19. Solid sample measurment using the integrating sphere method.
Source: Optional Accessories for Shimadzu UV-Vis spectrophotometers

3.4.4. Luminescence spectra

Solid samples were ground and pressed onto the silica window of a sample screw holder. Photoluminescence spectra were detected in range of 200-800 nm.

CHAPTER 4

RESULTS AND DISCUSSION

1. Synthesis of zinc oxide powders

In this work, three aminoalcohols: monoethanolamine, diethanolamine and triethanolamine were used as stabilizer or capping agent. Aminoalcohols are organic compound that contains both amine and alcohol functional groups. Regarding each aminoalcohol molecule, MEA is both primary amine and primary alcohol. When the one of hydrogen atom in MEA is substituted by $-CH_2CH_2OH$ group, it is known as DEA. TEA is formed if all hydrogen atoms in MEA are substituted with CH_2CH_2OH group as shown in figure 20.
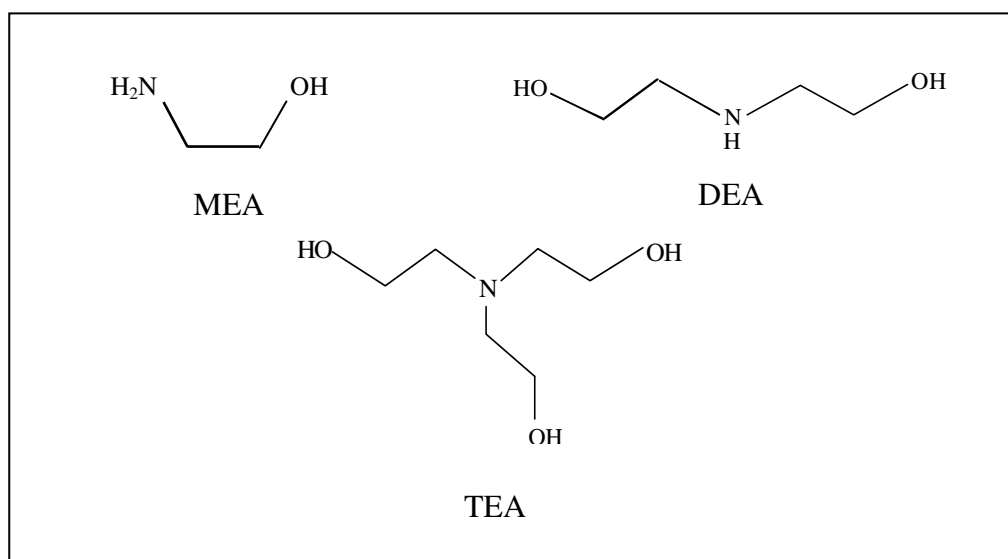
Figure 20. Structure of MEA, DEA and TEA molecules.

Source: http://en.wikipedia.org/wiki/File:Ethanolamine-2D-skeletal-B.png

Source: http://en.wikipedia.org/wiki/File:Diethanolamine.png

Source: http://en.wikipedia.org/wiki/File:Triethanolamine.png

In fact, these three aminoalcohols (MEA, DEA and TEA) act as a weak base like other amines, thus the OH$^-$ ions can be generated when they dissolve in aqueous solution as follow:

$$(CH_3CH_2OH)_nNH_{3-n} \; + \; H_2O \; \rightleftharpoons \; (CH_3CH_2OH)_nN^+H_{4-n} \; + OH^-$$
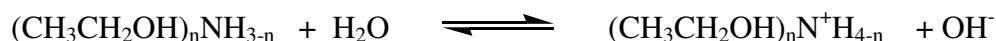
where n = 1-3 (n(MEA) = 1, n(DEA) = 2 and n(TEA) = 3). To study the effect of these capping agents on morphological change, the mole ratio of Zn^{2+}: aminoalcohol was first elucidated in detail and their ratios were depicted in table 4.

Table 4. Various mole ratios of Zn^{2+}: aminoalcohol.

aminoalcohol	mole ratio of Zn^{2+}: aminoalcohol	physical properties
-	1:0	white powder
MEA	1:1	faintly pinkish white powder
	1:2	faintly pinkish white powder
	1:3	faintly pinkish white powder
DEA	1:1	faintly pinkish white powder
	1:2	faintly pinkish white powder
	1:3	faintly pinkish white powder
TEA	1:1	faintly pinkish white powder
	1:2	faintly pinkish white powder
	1:3	faintly pinkish white powder

Zinc oxide (ZnO) powders were prepared through the reaction of Zn(NO$_3$)$_2$·6H$_2$O and NH$_4$OH solutions. In the crystallization process, the aminoalcohol was added into an aqueous Zn(NO$_3$)$_2$·6H$_2$O solution, giving rise to the

generation of OH$^-$ ions. These OH$^-$ ions could interact with Zn^{2+} ions to form the white Zn(OH)$_2$ precipitates in the solution. When the NH$_4$OH was then added dropwise into the mixture, the Zn(OH)$_2$ precipitates were dissolved and formed Zn(NH$_3$)$_4$$^{2+}$ species in the solution.

$$Zn^{2+} + 2OH^- \rightleftharpoons Zn(OH)_2$$

$$Zn^{2+} + 4NH_3 \rightleftharpoons Zn(NH_3)_4{}^{2+}$$

Jang *et al*., (2008) reported that Zn(NH$_3$)$_4$$^{2+}$ species can transform easily to Zn(OH)$_2$ at pH < 10. Then, the ZnO crystal growth can be occurred in a heterogeneous system. When the pH is more than 10.0, the Zn(OH)$_4$$^{2-}$ species formed though dissolution of Zn(OH)$_2$.

$$Zn(OH)_2 + 2OH^- \rightleftharpoons Zn(OH)_4{}^{2-}$$

If the temperature increased, ZnO nuclei could form from the dehydration of Zn(OH)$_4$$^{2-}$ ions and followed by crystal growth (Li *et al*., 2007).

$$Zn(OH)_4{}^{2-} \rightleftharpoons ZnO + 2H_2O + 2OH^-$$

Simultaneously, Zn(NH$_3$)$_4$$^{2+}$ can react with OH$^-$ ions to form ZnO as following reaction:

$$Zn(NH_3)_4{}^{2+} + 2OH^- \rightleftharpoons ZnO + 4NH_3 + H_2O$$

In this work, the mole ratio of Zn^{2+}: NH$_4$OH was kept constant at 1:2 and the pH value of solution was higher than 10.5. Under this considerable condition, the growth unit is assigned to Zn(OH)$_4$$^{2-}$ species.
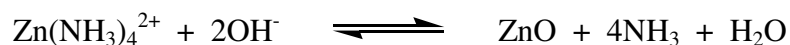
2. Characterization of zinc oxide powders

2.1. Phase identification

As we know, phase of materials strongly affects their properties. Therefore, a kind of present phase as well as its purity were first identified. The XRD technique is an easy method which use for phase identification of many materials. The diffraction patterns of all calcined powders prepared from various mole ratios of Zn^{2+} : aminoalcohol as described in table 4, are identical with the standard pattern of ZnO in JCPDS card number 36-1451 as shown in figure 21-23. These patterns are indexed to the heaxagonal or wurtzite structure with a space group $P6_3mc$. Moreover, entire ZnO powders synthesized from all conditions show a single phase without other detectable impurities or secondary crystalline phases in obtained XRD patterns.
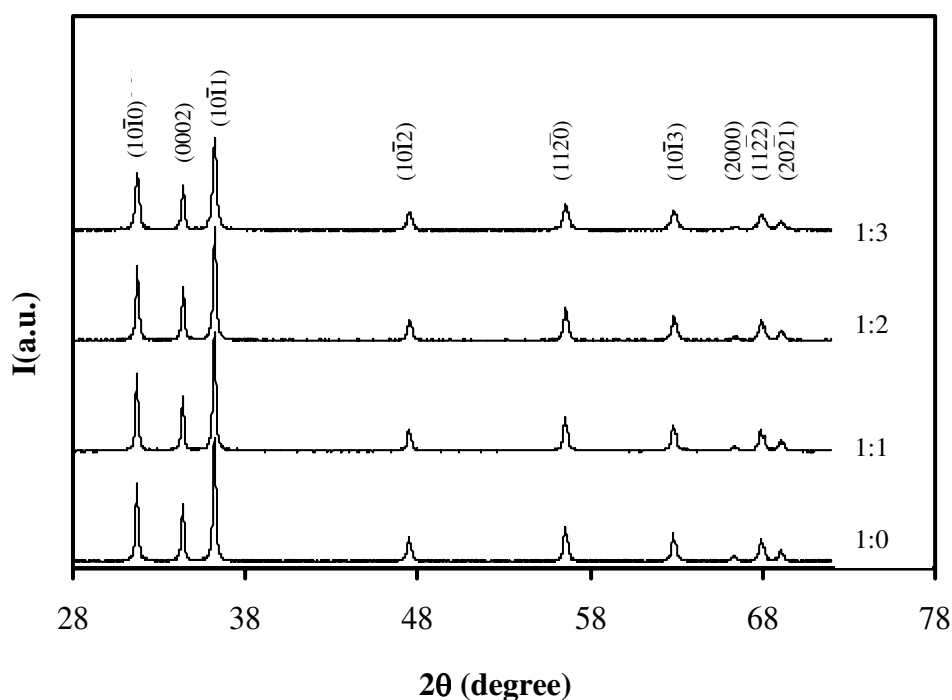
Figure 21. XRD patterns of ZnO powders prepared from different mole ratios of Zn^{2+}: MEA at 1:0, 1:1, 1:2 and 1:3.
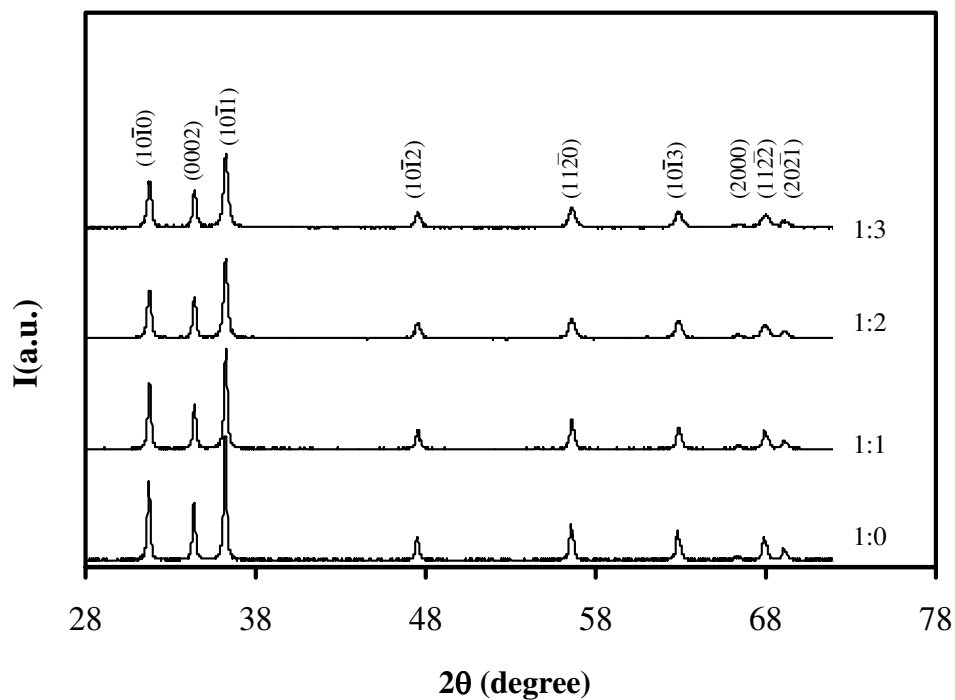
Figure 22. XRD patterns of ZnO powders prepared from different mole ratios of Zn^{2+}: DEA at 1:0, 1:1, 1:2 and 1:3.
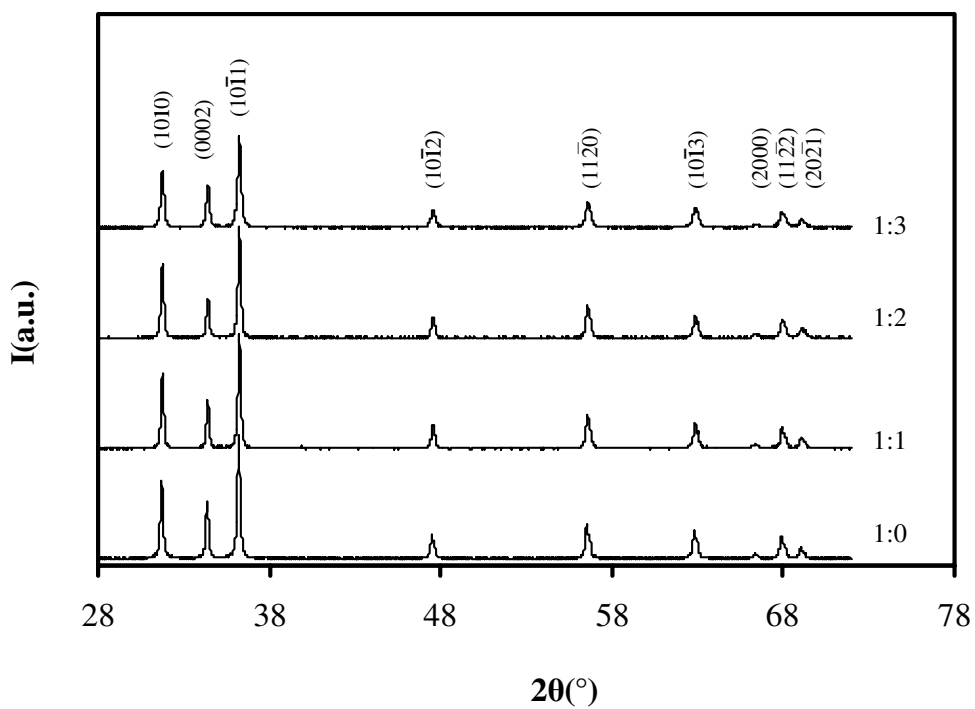

Figure 23. XRD patterns of ZnO powders prepared from different mole ratios of Zn^{2+}: TEA at 1:0, 1:1, 1:2 and 1:3.

Based on the XRD results presented in figure 21-23, its was observed that the ZnO powders obtained from all conditions have a good crystallinity. The crystallite size of all samples was calculated by the Scherrer equation (Weller, 1996):

$$D = \frac{0.9\lambda}{\beta \cos\theta}$$

where D is the average crystallite size (nm), λ is the wavelength of Cu K_α (0.15406 nm), θ is the Bragg angle and β is the full-width at half maximum (FWHM) in radian.

The average crystallite sizes estimated from the first five peaks for each sample are presented in table 5. From this result, the average crystallite sizes of all samples decreased as the mole ratios of Zn^{2+}: aminoalcohol were increased from 1:0 to 1:3.

Regarding the effect of each aminoalcohol molecule, MEA is both primary amine and primary alcohol. Therefore, when one or two hydrogen atoms in MEA is substituted by $-CH_2CH_2OH$ group, it is known as DEA or TEA, respectively. These aminoalcohols can serve as a surface modifier or capping agent and the aminoalcohol presumably interacts with the growth unit (usually refers to $Zn(OH)_2$ or $Zn(OH)_4^{2-}$, depending on pH) at Zn position by lone pair of N in aminoalcohol, resulting in the inhibition of crystal growth along c-axis, so the small rod was formed at higher concentration of aminoalcohols. In this study, the growth along c-axis was substantially retarded when the aminoalcohols concentrations increased and ZnO shape was changed to another stable form.

Table 5. Information of nanocrystalline ZnO powders prepared at various mole ratios
of Zn^{2+}: aminoalcohol.

sample code	stabilizers	mole ratio	crystallite size (nm)	E_g (eV)	particle shape
A	-	1:0	72.40 ± 1.20	3.208	large rod
B		1:1	68.67 ± 2.05	3.216	large rod + rice -like
C	MEA	1:2	52.00 ± 2.11	3.227	small rod + rice –like
D		1:3	39.66 ± 3.05	3.202	rice –like
E		1:1	58.15 ± 0.95	3.216	large rod + rice -like
F	DEA	1:2	52.06 ± 1.10	3.224	rice –like
G		1:3	43.35 ± 2.56	3.210	rice –like
H		1:1	62.13 ± 2.10	3.222	rod + rugby-like
I	TEA	1:2	59.25 ± 0.99	3.206	rugby–like
J		1:3	54.90 ± 2.04	3.184	sphere

2.2. Morphological study

From XRD result, the synthesized ZnO powders performed a single phase and their crystallite sizes are dependent upon the type and concentration of aminoalcohols. As a matter of fact, crystallite size is an imaginary domain even though it is not an actual particle size, it can be correlated to the particle size that can be observed by many techniques such as SEM and TEM, etc.

In this study, the morphology of nanocrystalline ZnO powders was examined with SEM. Figure 24 shows morphology of nanocrystalline ZnO powders obtained from studied conditions without any addition of aminoalcohols or capping agents. A typical large rod shape which is reported in publication (Wu *et al*., 2006) was observed in this study. However, the morphology of nanocrystalline ZnO powders prepared from different capping agents at various mole ratios of Zn^{2+}: capping agent show various shapes as seen in figure 25-27.

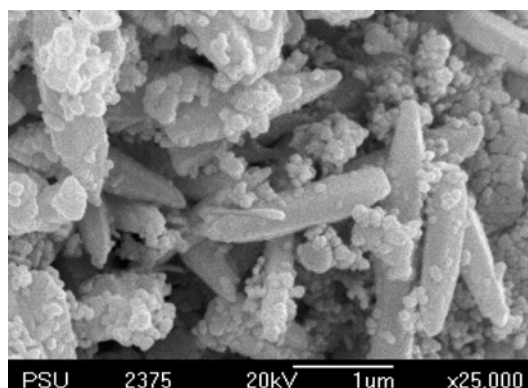
Figure 24. SEM image of ZnO powders.

Figure 25. SEM images of ZnO powders prepared at different mole ratios of Zn^{2+}: MEA (a) 1:1, (b) 1:2 and (c) 1:3.

Figure 26. SEM images of ZnO powders prepared at different mole ratios of Zn^{2+}: DEA (a) 1:1, (b) 1:2 and (c) 1:3.
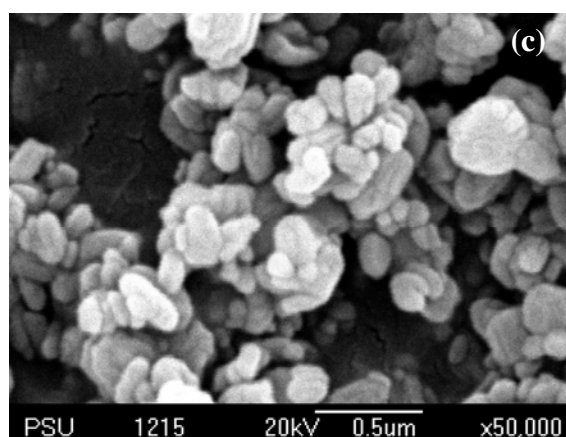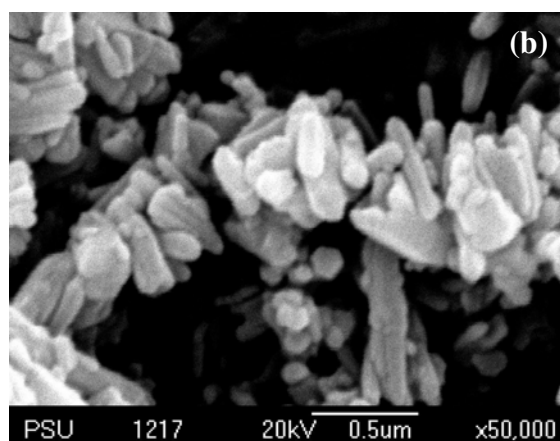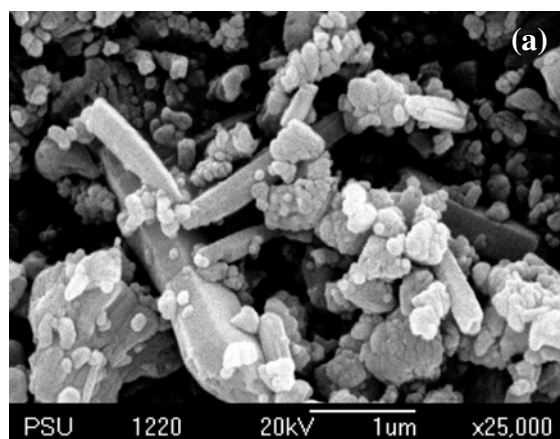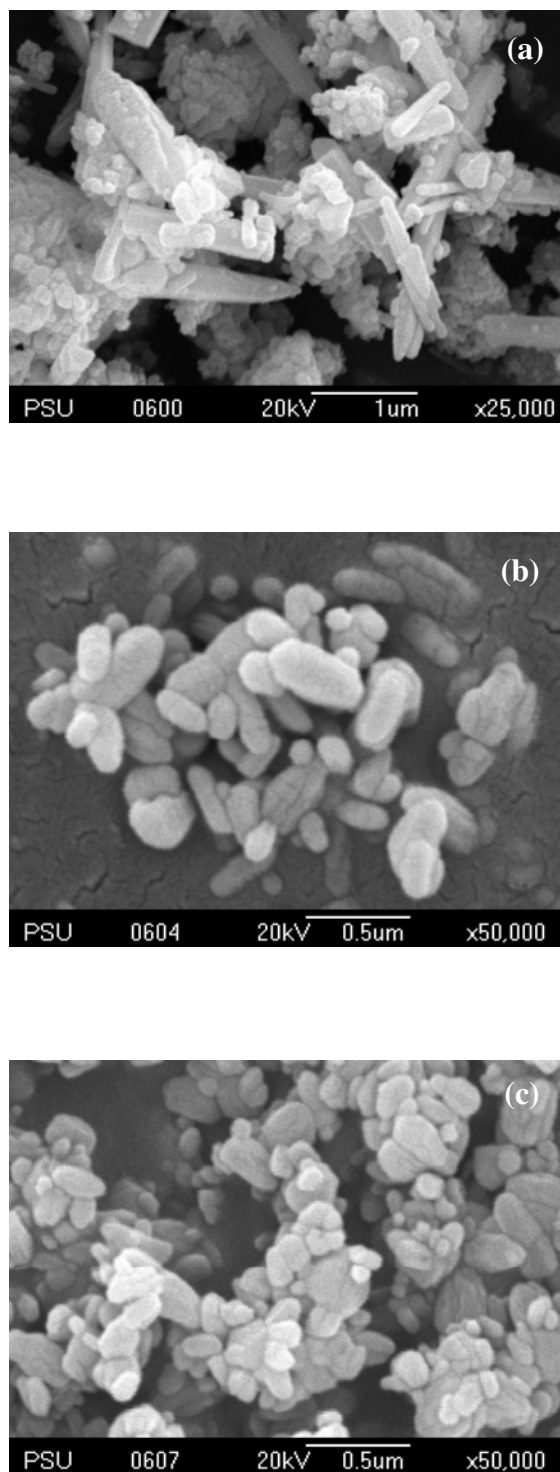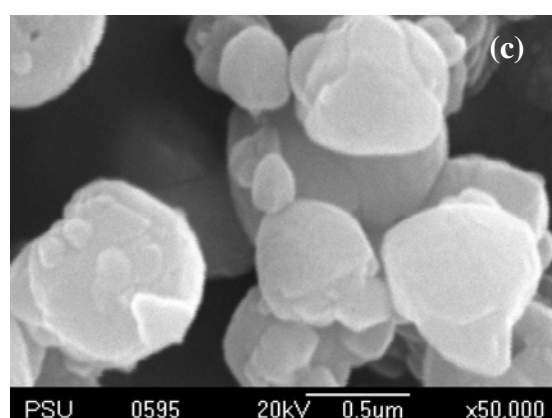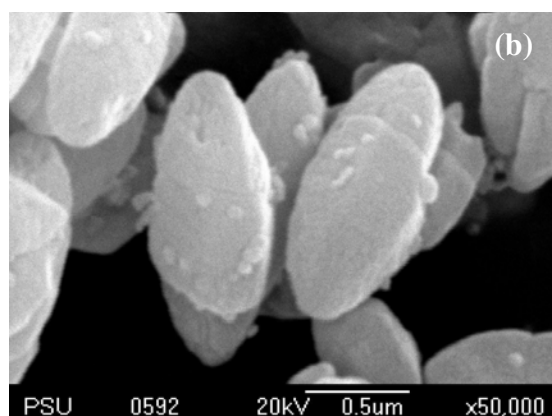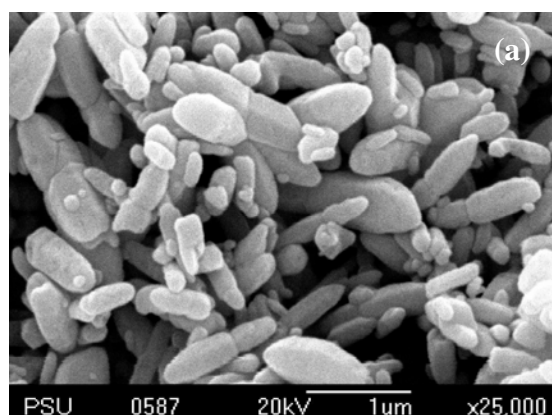
Figure 27. SEM images of ZnO powders prepared at different mole ratios of Zn^{2+}: TEA (a)1:1, (b) 1:2 and (c) 1:3.

It is evident that the similar morphology of ZnO powders is observed as MEA and DEA were utilized as capping agent. A mixture of large rod and rice-like structure was shaped at low concentration of MEA and DEA, whereas only rice-like shape was formed at high concentration. On the other hand, the shape of nanocrystalline ZnO powders was changed from rod-like to rugby-like shape and subsequently to spherical shape as TEA concentration was increased. Once again, the obtained crystallite size and the particle size of nanocrystalline ZnO powders prepared from MEA-, DEA- and TEA-modified $Zn(NO_3)_2 \cdot 6H_2O$ solution related to the amount of capping agent *i.e.* the crystallite size and particle size sysmatically decreased as capping agent was increased. The role of each capping agent in controlling the morphology of ZnO powders will be explained in detail later.

It is well known that ZnO is a polar crystal, whose polar axis is the *c*-axis, and consists of a positive polar (0001) plane rich in Zn^{2+} ions and a negative polar $(000\bar{1})$ plane rich in O^{2-} ions. In coordination structure of ZnO crystal, the coordination number of Zn is four; all the tetrahedrons are connected together by corner sharing. So, the terminal vertex of a cornor of coordination polyhedron can still bond with three growth unit. The orientation of the $Zn-O_4^{6-}$ tetrahedron in every sheet is obtained by rotating the adjacent sheet by 180º around the *c*-axis of the hexagonal lattices as shown in figure 28 (Li *et al*., 1999).
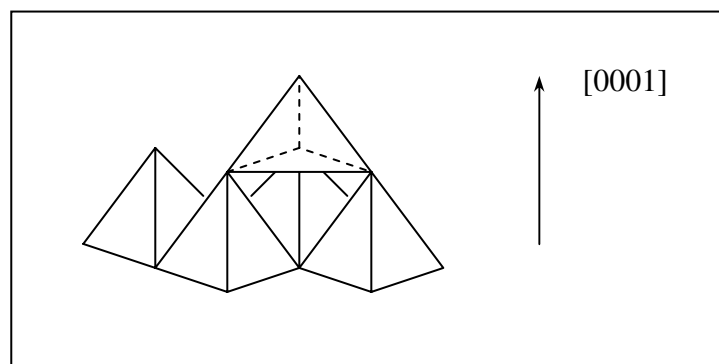
Figure 28. Idealized interface structure image of ZnO crystal in [0001] direction.
Source: Li *et al*., (1999)

Figure 28 shows that the terminal vertex of the cornor of the coordination of the polyhedron has the strongest bonding force, the terminal vertex of the edge of the coordination polyhedron has the second strongest binding force and the terminal vertex of face of the coordination polyhedron has the smallest binding force. So, the crystal force with the corner of the coordination polyhedron present at the interface has the fastest growth rate; the crystal face with the edge of the coordination polyhedron present at the interface has the second fastest growth rate and the crystal face with the face of coordination polyhedron present at the interface has the slowest growth rate. From this reason, the growth velocities in different directions are reported to be $V_{[0001]} > V_{[\bar{1}01\bar{1}]} > V_{[\bar{1}010]} > V_{[\bar{1}011]} > V_{[000\bar{1}]}$ when a hydrothermal route is employed (Hi *et al.*, 2005). Accordingly, the most stable crystal structure is a regular prismatic hexagonal elongated along the *c*-axis as seen in figure 29.
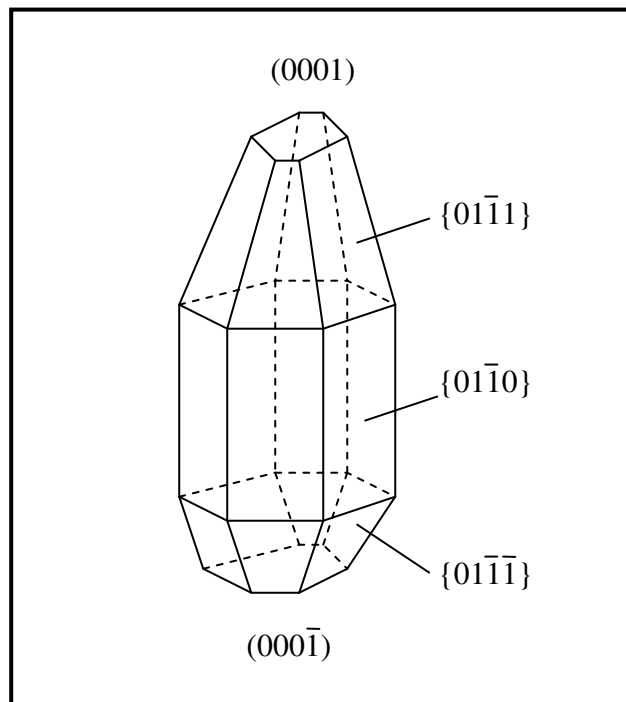
Figure 29. The facets in ZnO crystal.

Source: Li *et al.*, (1999)

Considering the ZnO powders gained from the conditions without addition of aminoalcohols, a large rod-like shape of ZnO powders was observed as shown in figure 24 owing to the fastest velocity of crystal growth in (0001) plane. The morphological change was observed when the aminoalcohol was added in the solution. As mentioned above, the aminoalcohol is a weak base and gives the OH$^-$ ions after its dissociation. But the ionic form is decreased in aqueous alkaline media by Le Chatelier's principle. In non-ionic form, aminoalcohol has a lone pair on the N atoms that can interact with cation link Zn^{2+} in ZnO during growing process. These capping agents may serve as a surface modifier and presumably bond to Zn^{2+} ions on the polar (0001) planes of ZnO crystal during the adsorption process when their concentrations were increased. This surface interaction inhibited an elongation of ZnO crystals along (0001) plane. However, the inherent anisotropic growth of ZnO crystals along c-axis is still favorable at low concentration of capping agent, thus the small rod or rice-like ZnO powders was shaped when using MEA, DEA and TEA as capping agent as clearly seen in figure 25 (b), 26 (b) and 27 (b), respectively. In this study, the growth along c-axis substantially retarded when the capping agent concentrations increased and morphology of ZnO powders was changed to another favorable shape that occupies low energy and stable form because the shape formation depends on the nature of capping agent and adsorbing direction on ZnO particles.

Taking into account the geometrical structure of MEA, DEA and TEA molecule, the number of substituted $-CH_2CH_2OH$ group or a chain size brought about the molecules to have a dynamic volume increasingly (TEA > DEA > MEA) and gave more repulsive force or steric effect when the capping agent molecules got close to another one. As a result of three substituted groups, TEA is the biggest molecule. Therefore, if the capping agent absorbed on (0001) plane of ZnO, TEA molecule would spread and branch out to encapsulate the (0001) plane of ZnO particle with a larger surface area comparing to MEA and DEA as presented in figure 30. This effect is known as steric effect. ZnO powders then growed along a-axis or in prism plane. The steric effect occurred predominantly in the case of TEA used when regarding at the same mole ratio of Zn^{2+}: capping agent each, giving rise to lateral growth mostly.
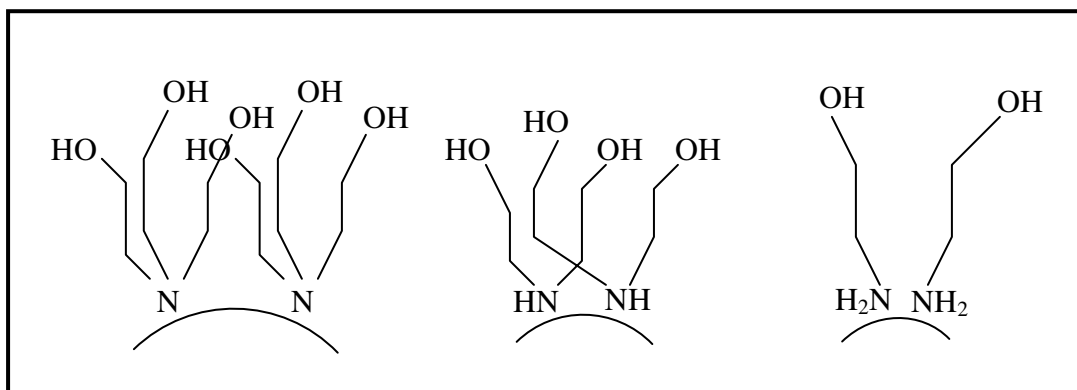
Figure 30. Absorbed illustration of aminoalcohols on (0001) plane of ZnO

In addition, in case of MEA and DEA used, mixture of big rod-like and rice-like ZnO shape was observed at low capping agent concentration. If the concentration of MEA and DEA is too low, they cannot throughout absorb or encapsulate on (0001) plane of all ZnO nuclei, then some ZnO nuclei can still grow in *c*-axis to form a big rod-like ZnO shape as seen in figure 25 (a) and 26 (a). However, some ZnO nuclei which were absorbed throughout the surface with MEA and DEA, formed a rice-like shape owing to the inhibition of crystal growth along (0001) plane. It was obviously seen that the big rod-like shape disappeared and only rice-like shape is observed (Figure 25 (c) and 26 (c)) by retarding the growth along *c*-axis when concentrations of MEA and DEA were increased.

On the contrary, if TEA molecules absorbed on ZnO nuclei, they could throughout absorbed on (0001) plane of ZnO nuclei due to its more steric effect. Therefore, the repulsion between TEA molecules increased and these molecules tried to rearrange an absorption model to spherical shape so as to reduce the repulsive force and make a system in equilibrium.

3. Optical properties

The unique and fascinating properties of nanostructured materials have triggered tremendous motivation among scientists to explore the possibilities of using them in technological applications. In particular, the optical properties of nanostructured materials have been interesting because of its great potential

applications in the fabrication of micro electronic and optoelectronic devices (Caglar *et al.,* 2009). ZnO is an important luminescent material due to a wide band gap (3.37 eV) and large excitation binding energy (60 meV) (Cheng *et al*., 2008). Moreover, it can be used to photodetectors operating in the UV region (Chen *et al*., 2009), light-emitting devices and semiconductor lasers (Hwangbo *et al*., 2008).

3.1. Band gap estimation

To estimate the band gap value, the absorbance characteristic of nanocrystalline ZnO powders prepared from the solutions modifying with three aminoalcohols were investigated by UV-Vis spectrophotometer by diffuse reflectance method. The absorbance behavior was measured as a function of wavelength in the range of 200-800 nm. All calcined ZnO powders showed a highly transparent mode in visible region as shown in figure 31-33.
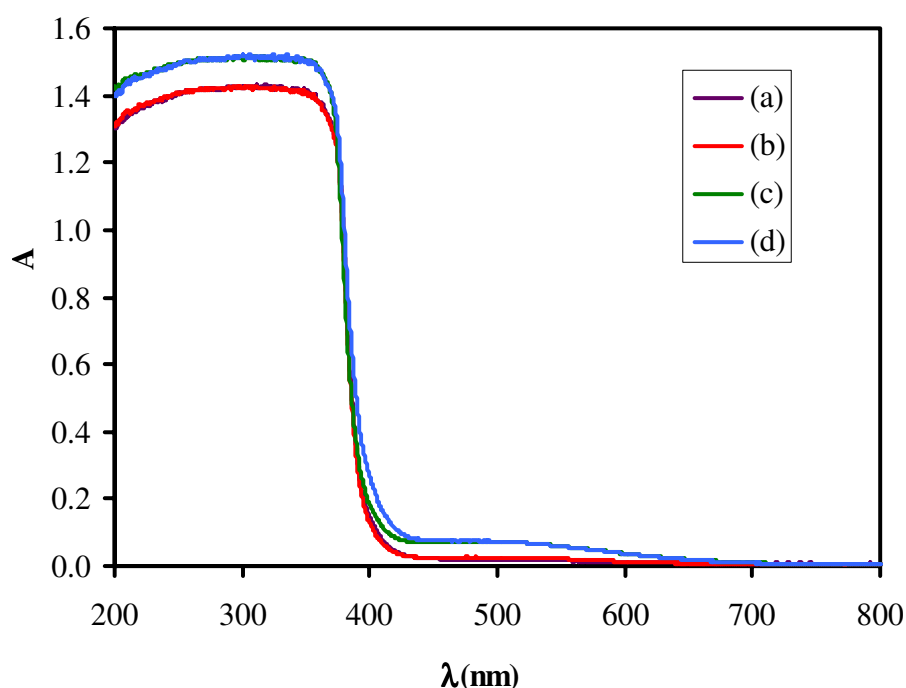
Figure 31. Absorption spectra of ZnO powders prepared at different mole ratios of Zn^{2+}: MEA, (a) 1:0, (b) 1:1, (c) 1:2 and (d) 1:3.
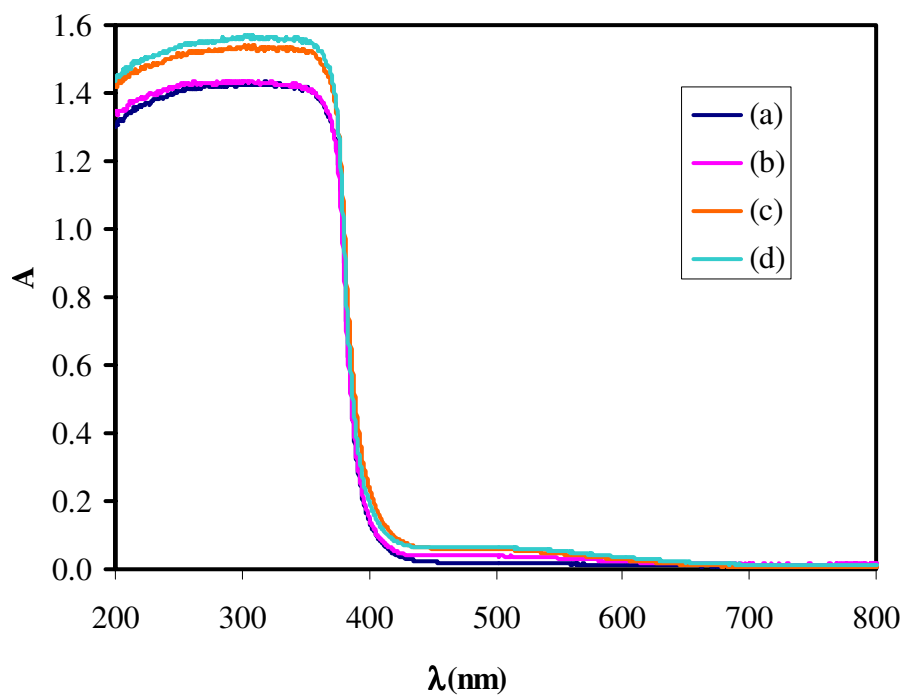
Figure 32. Absorption spectra of ZnO powders prepared at different mole ratios of Zn^{2+}: DEA, (a) 1: 0, (b) 1: 1, (c) 1: 2 and (d) 1: 3.
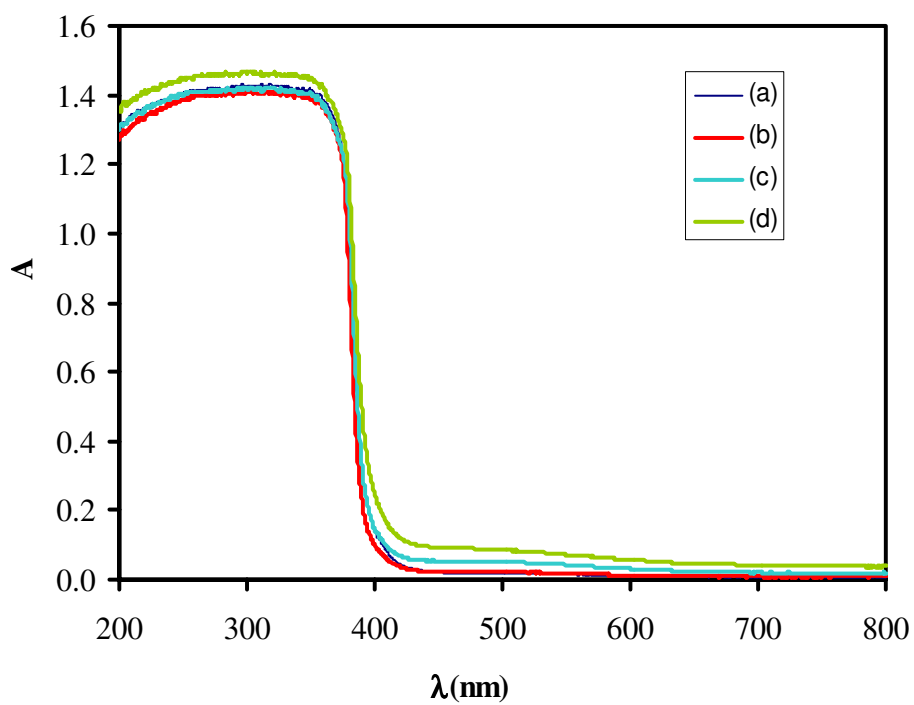
Figure 33. Absorption spectra of ZnO powders prepared at different mole ratios of Zn^{2+}: TEA, (a) 1:0, (b) 1:1, (c) 1:2 and (d) 1:3.

Based on the absorption spectra, the direct band gap of nanocrystalline ZnO powders could be estimated from the relationship as follow: (Serpone *et al.*, 1995)

$$(\alpha h\nu)^2 = E_D(h\nu - E_g)$$

where α is the optical absorption coefficient, h is the Planck's constant, ν is the frequency of the incident photon, E_D is the constant and E_g is the direct band gap. In general, the absorption coefficient (α) could be evaluated by the following equation.

$$\alpha = \frac{A}{d_s^{/}}$$

where A is the measured absorbance and $d_s^{/}$ is the thickness of samples in the UV-vis cell (0.4 cm), and $E(h\nu)$ or photon energy could be approximated by

$$E = h\nu = \frac{1240}{\lambda}$$

where λ is the measured wavelength in nm.

Figure 34-36 show the graph of $(\alpha h\nu)^2$ versus $h\nu$ for all nanocrystalline ZnO powders obtaining in this study. The values of direct band gap obtained from the linear portion of the curves were presented in table 5.
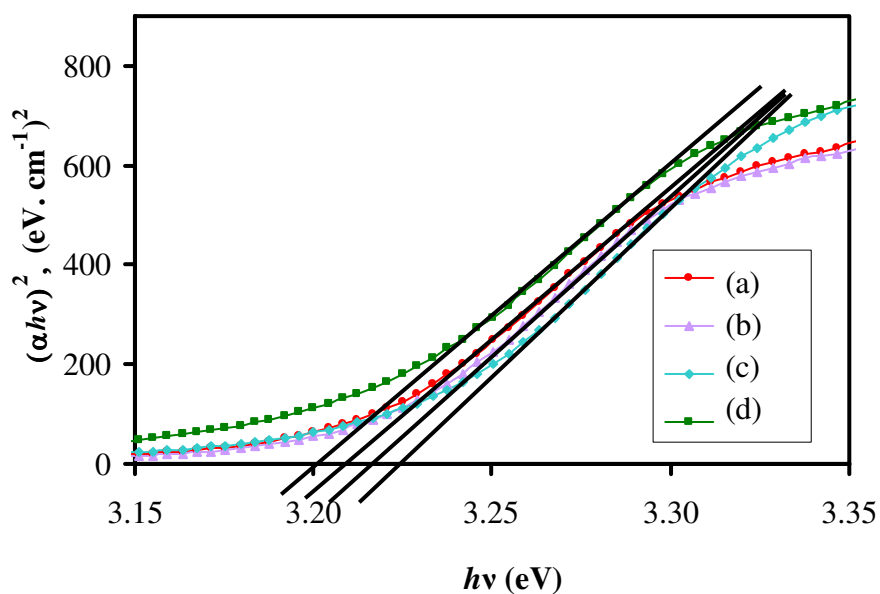
Figure 34. Plots of $(\alpha h\nu)^2$ versus $h\nu$ for nanocrystalline ZnO powders prepared at various mole ratios of Zn^{2+}: MEA, (a) 1: 0, (b) 1: 1, (c) 1: 2 and (d) 1: 3.
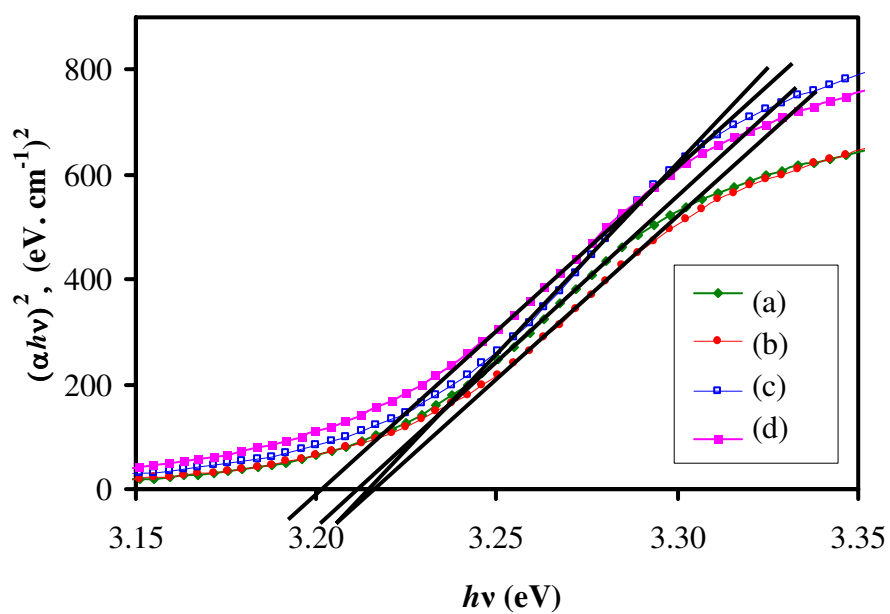
Figure 35. Plots of $(\alpha h\nu)^2$ versus $h\nu$ for nanocrystalline ZnO powders prepared at various mole ratios of Zn^{2+}: DEA, (a) 1: 0, (b) 1: 1, (c) 1: 2 and (d) 1: 3.
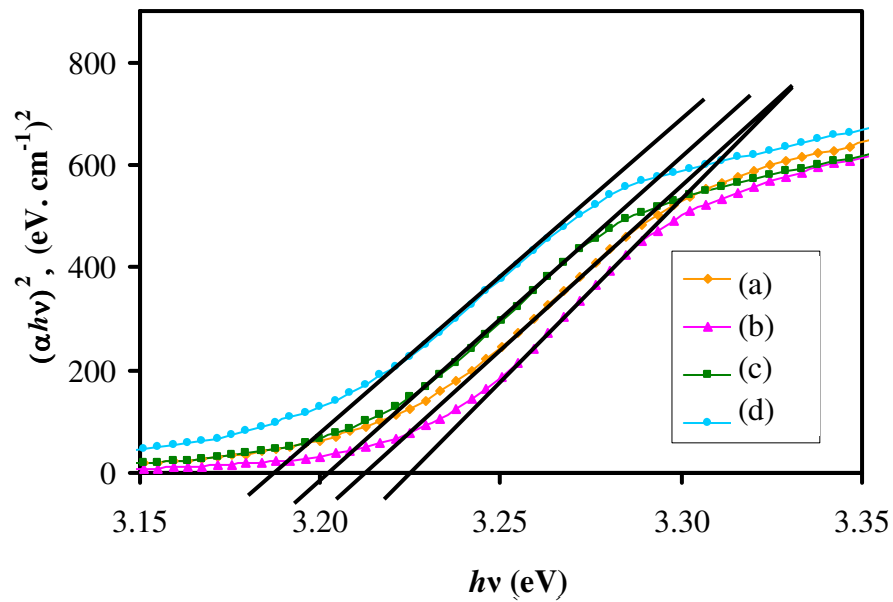
Figure 36. Plots of $(\alpha h\nu)^2$ versus $h\nu$ for nanocrystalline ZnO powders prepared at various mole ratios of Zn^{2+}: TEA, (a) 1: 0, (b) 1: 1, (c) 1: 2 and (d) 1: 3.

It is well-known that the UV absorption of ZnO powders related to the electronic transition from filled valence states to empty conduction states and the optical band gap can be defined as the difference between the valence band and conduction band in momentum space. As a matter of fact, the optical band gap energy is directly dependent upon particle shape and particle size. Thus, we will discuss these two parameters in this section.

Regarding the E_g values of the powders prepared from MEA-modified $Zn(NO_3)_2 \cdot 6H_2O$ solutions. The E_g values increased from 3.208 to 3.216 and 3.227 eV as the MEA concentration or the mole ratio of Zn^{2+}: MEA was increased from 1:0 to 1:1 and 1:2, respectively. Similarly, the E_g values of ZnO powders prepared from DEA-modified $Zn(NO_3) \cdot 6H_2O$ solutions increased from 3.208 to 3.216 and 3.224 eV as a mole ratio of Zn^{2+}: DEA was increased from 1:0 to 1:1 and 1:2, respectively. This can be explained by the modification of the band structure, i.e; narrowing of the valence band and conduction band. Thus, the smaller crystallite size performed the larger band gap. Nevertheless, the E_g value of ZnO powders decreased again if the

mole ratio of Zn^{2+}: MEA and Zn^{2+}: DEA was 1:3 even though the crystallite size of the samples still decreased systematically. The red-shift or decrease of E_g is caused by the increase of defects or oxygen vacancies, insisting by the luminescent characteristic that will be mentioned in detail in next section.

The E_g values of ZnO powders prepared from TEA-modified $Zn(NO_3)_2 \cdot 6H_2O$ solutions decreased from 3.222 to 3.206 and 3.184 eV as the mole ratio of Zn^{2+}: TEA was increased from 1:1 to 1:2 and 1:3, respectively. It is noteworthy that the red-shift occurred even though the crystallite size was decreased. In this study, the reduction of the E_g values or red-shift in the band gap could be explained by the enhancement of oxygen vacancies (Dutta *et al*., 2007) that were numerously created in calcined ZnO powders. It is to be noted that the defects or the nature of disorder in the system brought about the localized energy level inside the band gap or discrete states. This is well-known for band tailing effect (Dutta *et al*., 2007). In general, the absorption coefficient just below the band edge ($E < E_g$) should vary exponentially with photon energy according to the relationship:

$$\alpha E \ = \ \alpha_0 \exp (E/E_0)$$

where α_0 is a constant and E_0 is an empirical parameter depending on the defect concentration, temperature and structural disorder. The E_0 could be evaluated from the reciprocal of the slope of the linear part from the $\ln(\alpha)$ versus E curve ($E < E_g$) as presented in figure 37.
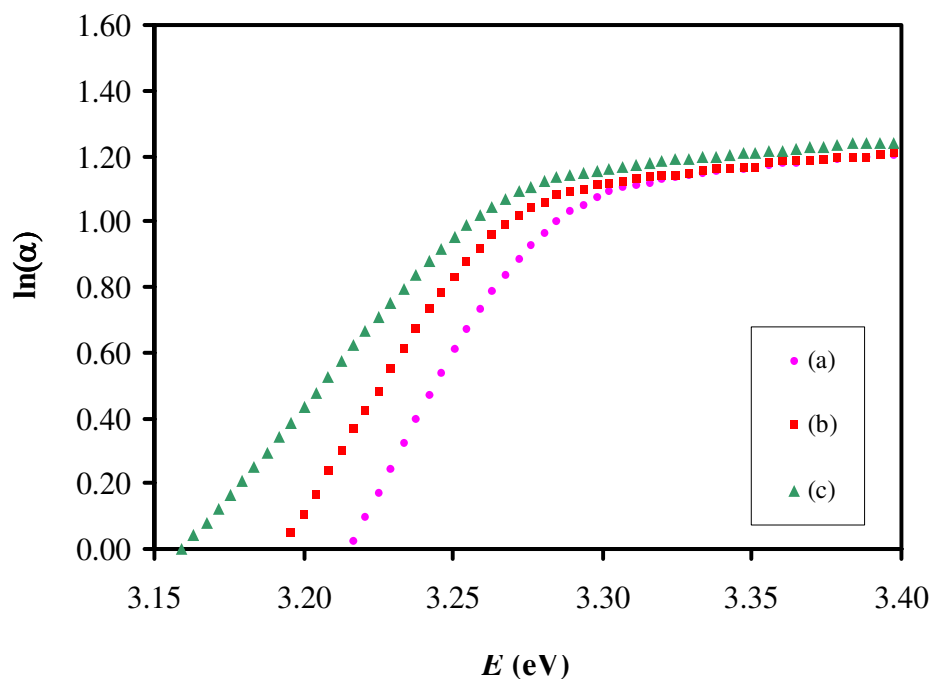
Figure 37. Plots of ln(α) versus photon energy for ZnO powders prepared at different

mole ratio of Zn^{2+}: TEA (a) 1:1, (b) 1:2 and (c) 1:3.

It is clearly seen that the obtained reciprocal slope increased from 0.059 to 0.075 and 0.095 as the mole ratio of Zn^{2+}: TEA was increased from (a) 1:1 to (b) 1:2 and (c) 1:3, respectively. Observing the morphology of ZnO powders again, the particle shape was significant changed from rod-like to rugby-like and spherical-like shape as a function of TEA concentration. Thus, we could also probably summarize that the different morphology has different level of defect concentration.

3.2. Emission spectra

Luminescence is a nonequilibrium process that needs excitation source, such as lamp or laser. As we know, photoluminescence (PL) which require optical excitation is one of the most widely used experimental methods for study of semiconductors, especially wide-band-gap materials. Generally, PL is devided into two major types: intrinsic and extrinsic luminescence.

The intrinsic luminescence is band-to-band luminescence, exciton luminescence and cross-luminescence. The recombination of an electron in the conduction band with a hole in the valence band generates band-to-band transition luminescence.

The extrinsic luminescence is normally generated by the impurities which are intentionally or unintentionally incorporated. These impurities are normally called activators.

In this section, we investigated the photoluminescence characteristic in ZnO powders.

In fact, the ZnO has an emission in a visible region whose it usually uses as light emitting diodes. The emission in ZnO comes from many partways as mentioned in Chapter 1. Therefore, the emission characteristic and the emission intensity of nanocrystalline ZnO powders prepared from solution modifying with three aminoalcohols were investigated by photoluminescence spectrophotometer with diffuse reflectance method at room temperature. The emission intensity was measured as a function of wavelength in the range of 200-800 nm. Comparison of the room temperature PL spectra for nanocrystalline ZnO powders prepared from different types and concentrations of aminoalcohol are presented in figure 38-40. It is obvious that the entire PL spectra show two emission peaks. The UV emission centered at about 390 nm is well understood as being the near-band-edge emission, whereas the broad visible emission originated from a variety of deep level defects, e.g. oxygen vacancies and zinc interstitials (Sun *et al*., 2006).

The nanocrystalline ZnO powders prepared from MEA-, DEA- and TEA- modified zinc nitrate solutions show the same evidence. The intensity of emissions in visible region decreased as MEA, DEA and TEA concentrations were

increased. Increasing of aminoalcohol concentrations, it can be indicated that their surface areas should be increased by the reduction of particle size of nanocrystalline ZnO powders as shown in figure 25-26. Based on the theory of physical chemistry of solid surfaces, particles with a large surface area to volume ratio have numerous draggling bonds and defects on its surface, that can absorb the O^{2-} and O^- to form an O^{2-}/O^- surface system. The O^{2-}/O^- surface system is the main trapper of the holes in the valence band, and plays an important role in the formation of oxygen vacancies. Thus the PL intensity increased because of a higher fraction of oxygen vacancies. Using MEA and DEA as capping agent, the intensity of emission was little changed however the significant increase of emission was observed in the nanocrystalline ZnO powders prepared from TEA-assisted zinc nitrate solution. This evidence might be come from the morphological change. In case of MEA and DEA used, the similar shape (large rod-like to small rice-like shape) was formed. On the other hand, TEA is a strong capping agent that can affect the ZnO morphological change (large-rod like shape to rugby-like shape and to spherical-like shape) and the distinctive change (TEA used) may be strong influenced from surface area of ZnO powders then the emission intensity increased significally comparing to the nanocrystalline ZnO powders prepared from MEA- and DEA- modified zinc nitrate solutions.
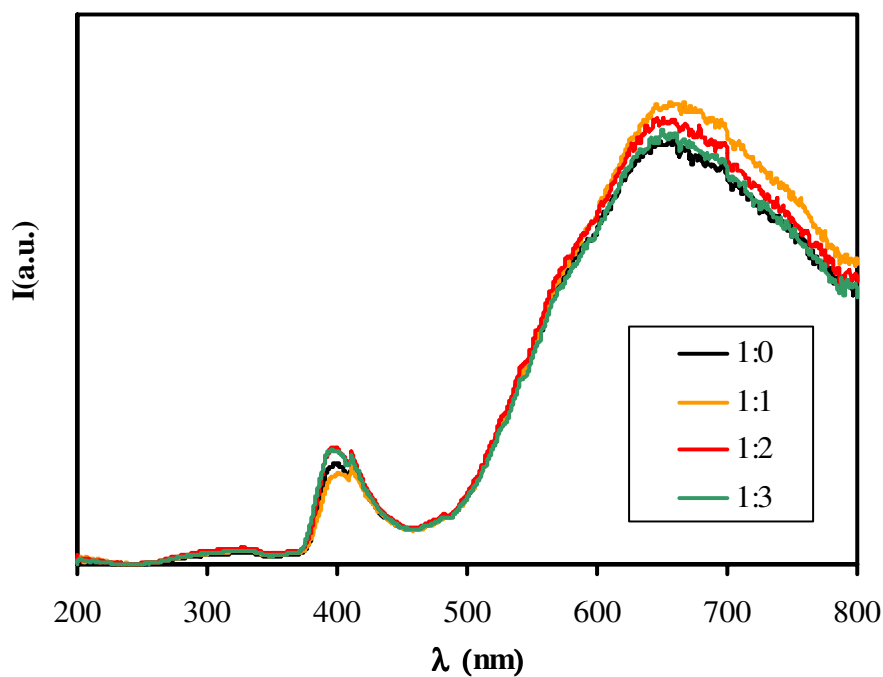
Figure 38. Room temperature PL spectra for nanocrystalline ZnO powders prepared from different mole ratios of MEA: Zn^{2+}.
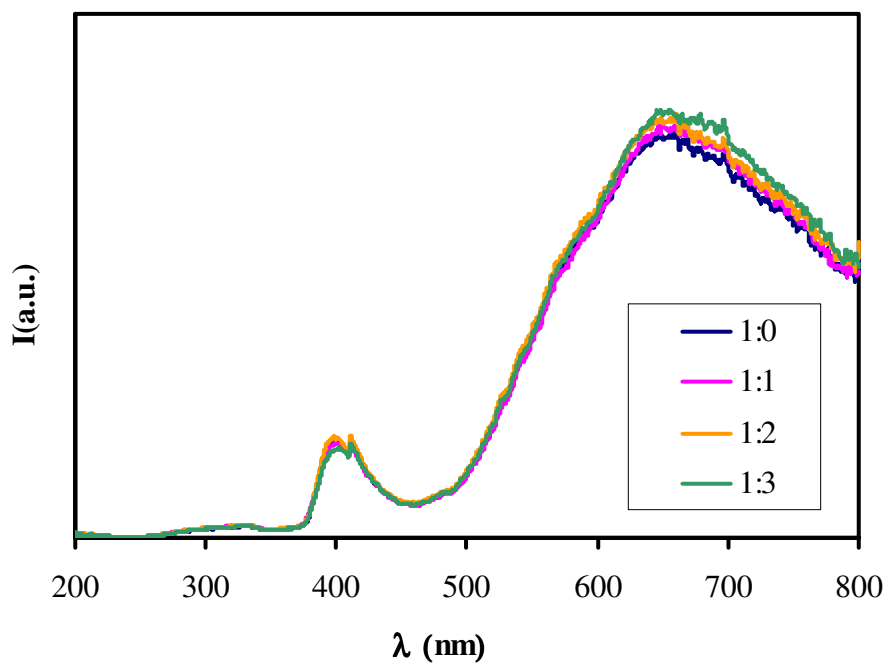
Figure 39. Room temperature PL spectra for nanocrystalline ZnO powders prepared from different mole ratios of DEA: Zn^{2+}.
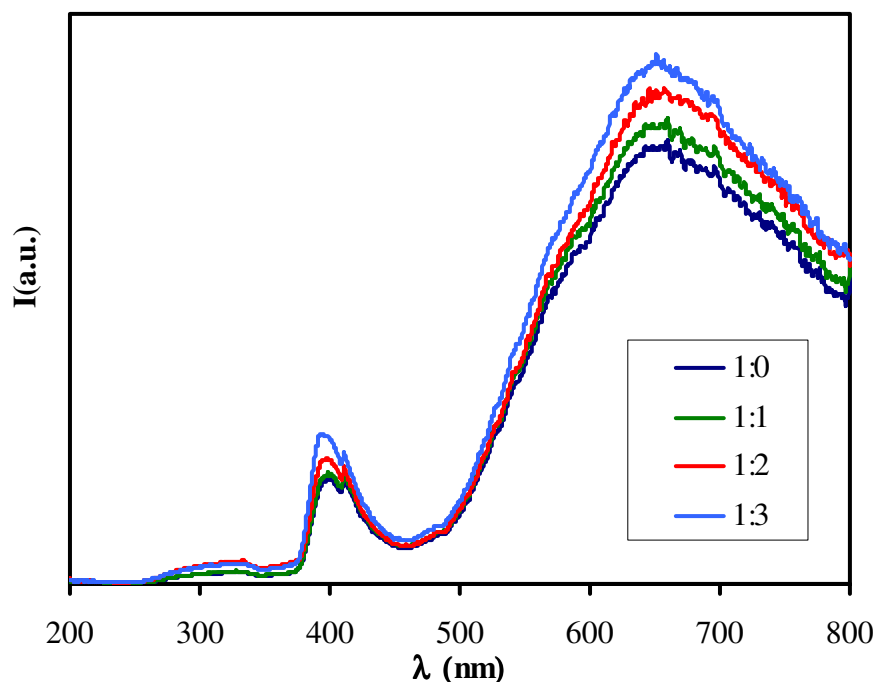
Figure 40. Room temperature PL spectra for nanocrystalline ZnO powders prepared
from different mole ratios of TEA: Zn^{2+}.

.

4. Photocatalytic activity

Photocatalytic degradation for dyes and organic compounds is the characteristic property that can be found in the metal oxide group such as TiO_2, ZnO and SnO_2 etc. In this study, we try to use the prepared ZnO powders for photocatalytic degradation of methylene blue (MB) dye under UV light. The absorption spectrum of MB in water as a stock solution is obtained in figure 41 that shows the maximum peak is about 655 nm. In order to investigate the photocatalytic activities of prepared ZnO powders, 100 mg of ZnO powders were added in 150 mL of 1.0×10^{-5} M MB solution. The UV source used in this work was the 2×18 watt blacklight tube, which emits UV light in the range 315-400 nm with a maximum at 352 nm and 368 nm.
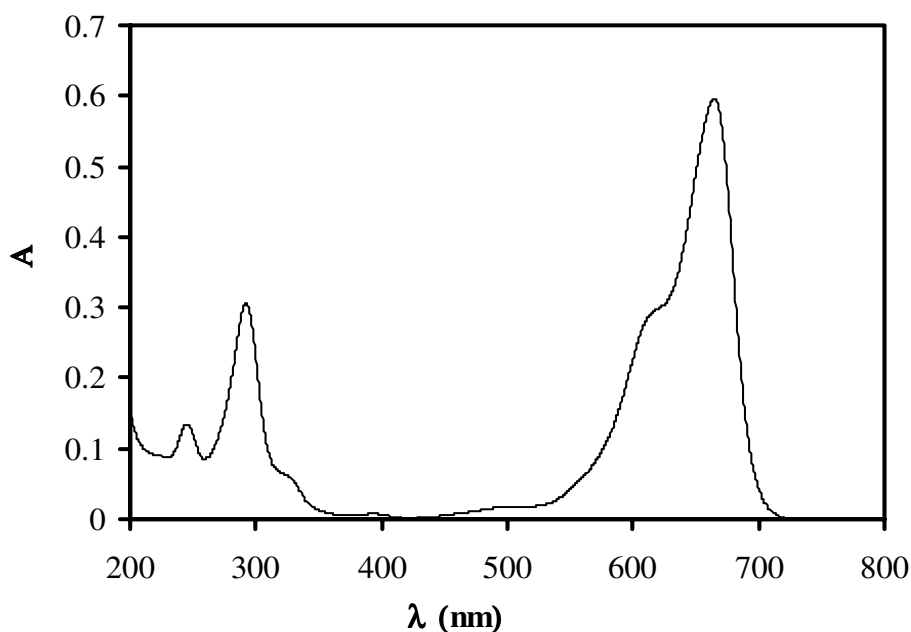
Figure 41. Absorption spectrum of 1.0×10^{-5} M MB in water.

Like dyes, the MB can be adsorbed on the surface of ZnO particles. To eliminate the error that come from adsorption ability of MB, the mixed solution (ZnO + MB solution) was stirred for 1 h under no UV irradiation. This effect can be confirmed by the decrease of its absorbance as shown in figure 42-45. After this stage, the adsorption/desorption are in equilibrium and a decrease in absorbance is not come from this mechanism. The photocatalytic degradation for MB at different irradiation time was monitored by a decrease in absorbance at 655 nm as shown in figure 46. Althrough the aminoalcohol modified-ZnO powders can be degrade the dye molecules under UV irradiation, they have lower photo catalytic efficiency than that prepared ZnO without aminoalcohol.
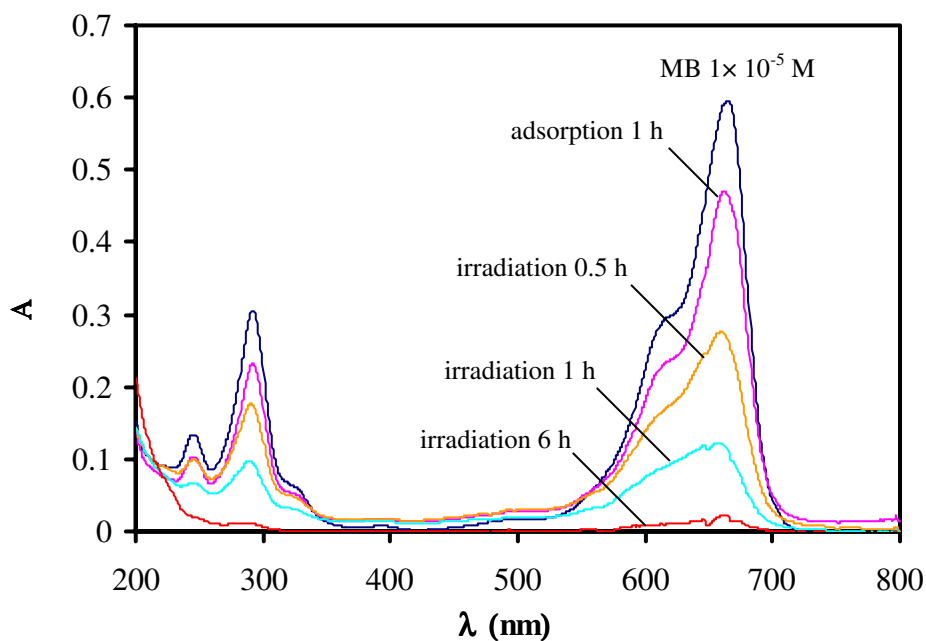
Figure 42. The UV-Vis spectral change of MB in prepared ZnO suspension when ZnO powders as a function of irradiation time.
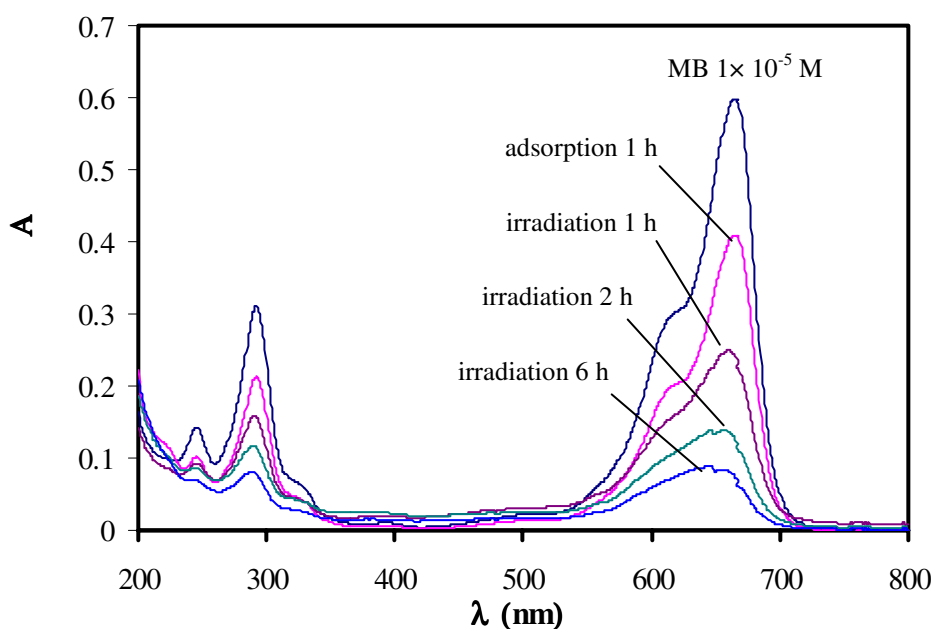
Figure 43. The UV-Vis spectral change of MB in prepared ZnO suspension when ZnO powders were prepared from MEA- modified Zn^{2+} solution, as a function of irradiation time.
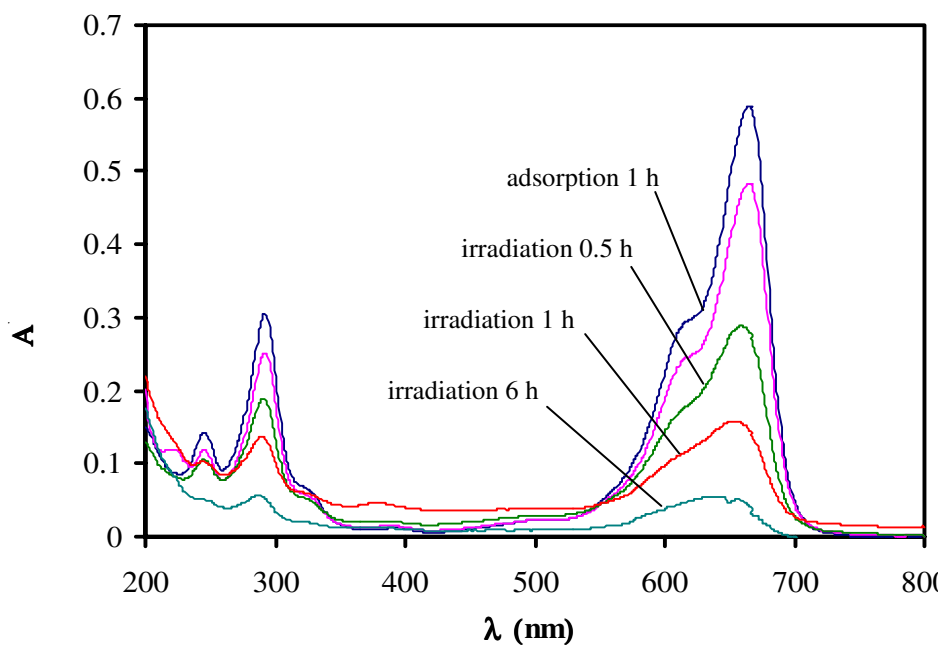
Figure 44. The UV-Vis spectral change of MB in prepared ZnO suspension when ZnO powders were prepared from DEA- modified Zn^{2+} solution, as a function of irradiation time.
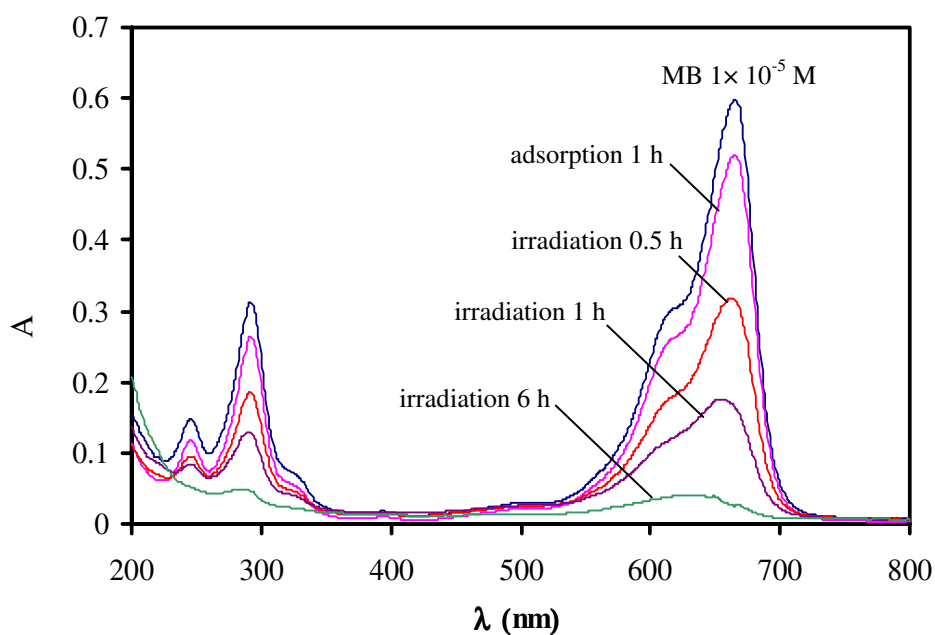
Figure 45. The UV-Vis spectral change of MB in prepared ZnO suspension when ZnO powders were prepared from TEA- modified Zn^{2+} solution, as a function of irradiation time.
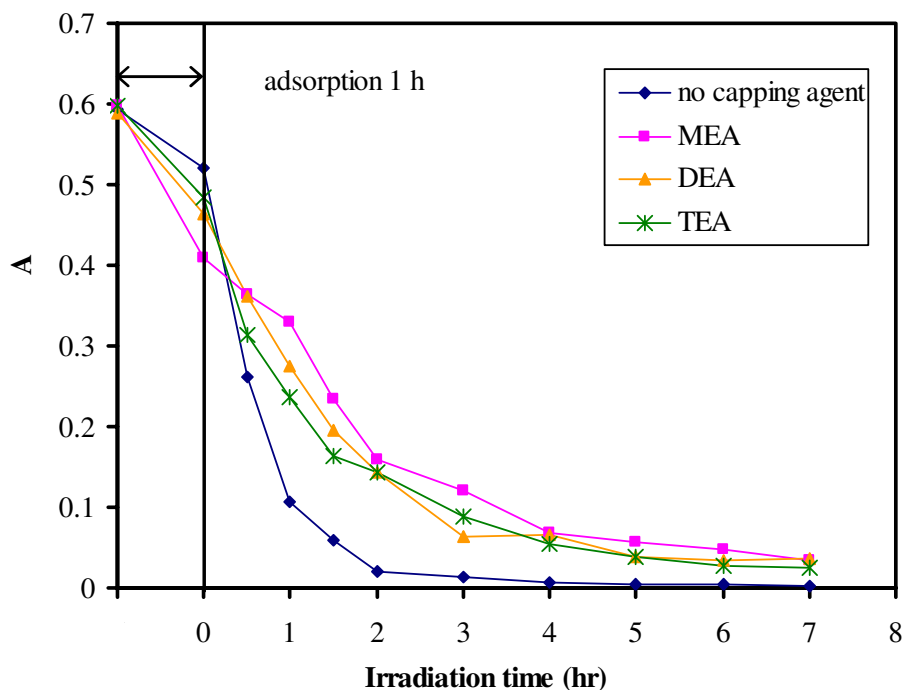
Figure 46. The remained absorbance of MB in prepared suspension as a function of irradiation time as the ZnO powders prepared from different capping agents modified Zn^{2+} solution with a mole ratio of 1:3 were used.

The absorption ability of MB on ZnO is in order: ZnO (MEA used) > ZnO (DEA used) > ZnO (TEA used) > ZnO (no aminoalcohol) that correspond to their particle size and crystallite size. ZnO that was prepared from MEA Zn^{2+} has the smallest particle size so its surface area must be the highest, Thus the highest amount of MB could be adsorbed. But the ZnO prepared from Zn^{2+} solution without addition of aminoalcohol has the largest particle size so it has smallest surface area, the smallest absorption ability of MB on ZnO powder was observed.

CHAPTER 5

CONCLUSIONS

Zinc oxide (ZnO) powders were prepared by hydrolysis of $Zn(NO_3)_2 \cdot 6H_2O$ in presence of NH_4OH solution and three aminoalcohols; monoethanolamine, diethanolamine and triethanolamine that acted as capping agents. The calcined ZnO powders were characterized by X-ray powder diffraction (XRD) techniques and scanning electron microscope (SEM).

The diffraction patterns of all calcined ZnO powders indexed heaxagonal or wurtzite structure with a space group *P6₃mc* corresponding to JCPDS file 36-1451 without other detectable impurity or secondary phase in XRD patterns. The average crystallite size for each sample decreased as a concentration of aminoalcohols was increased. The various shapes of nanocrystalline ZnO powders prepared from different capping agents at various mole ratios of Zn^{2+}: capping agent was observed. The favorable formation of particle shape was dependent on a kind of aminoalcohols. MEA and DEA showed similar result, the big rod was altered to small rod and rice-like shape as a function of MEA and DEA concentration. On the contrary, the particle shape was changed from rod to spherical shape as increasing in TEA concentration. The reasons can be attributed to steric effect of TEA and basicity of the solutions, which may influence the nucleation of ZnO nuclei and subsequently growth processes.

All calcined ZnO powders show a highly transparent mode in visible region. The strong influence of morphological modification is obtained in ZnO that was used TEA as capping agent, and the red shift is stronger than that of the others. The energy band gap may be significantly dependent on the shape of ZnO.

The nanocrystalline ZnO powders show a strong UV band emission centered at 390 nm. The intensity of emissions in visible region decreased as a function of MEA, DEA and TEA concentration. By increasing in aminoalcohol concentration, it can be indicated that their surface areas should be increased by a decrease of its particle sizes. By using MEA and DEA as capping agent, the emission

intensity was little changed however the significant increase of emission was observed in ZnO prepared by TEA-modified Zn^{2+} solution.

The absorption spectrum of MB in water shows the maximum intensity at about 655 nm. The ability of the MB was adsorbed on the ZnO to be in order: ZnO (MEA used) > ZnO (DEA used) > ZnO (TEA used) > ZnO (no aminoalcohol) that correspond to its particle size and crystallite size. However, all aminoalcohol modified-ZnO sample have lower photocatalytic efficiency than that ZnO powder without capping agent.

REFERENCES

Bahnajady, M.A., Modirshahla, N. and Hamzavi, R. 2006. Kinetic study on photocatalytic degradation of C.I. Acid Yellow 23 by ZnO photocatalyst. Journal of Hazardous Materials B. 133: 226–232.

Cao, G. 2004. Nanostructures & Nanomaterials: Synthesis. Properties & applications. Imperial College Press, London.UK.

Caglar, M., Ilican, S., Caglar, Y. and Yakuphanoglu, F. 2009. Electrical conductivity and optical properties of ZnO nanostructured thin film. Applied Surface Science. 255 : 4491–4496.

Chakrabarti, S. and Dutta, B. K. 2004. Photocatalytic degradation of model textile dyes in wastewater using ZnO as semiconductor catalyst. Journal of Hazardous Materials B. 112: 269–278

Chen, C., Liu, P. and Lu, C. H. 2008. Synthesis and characterization of nano-sized ZnO powders by direct precipitation method. Chemical Engineering Journal 144: 509–513.

Chen, K.J., Hung, F.Y., Chang, S.J. and Young, S. J. 2009. Optoelectronic characteristics of UV photodetector based on ZnO nanowire thin films. Journal of Alloys and Compounds xxx: xxx–xxx.

Cheng, B., Wang, X., Liu, L. and Guo, L. 2008. Growth mechanism and morphology dependent luminescence properties of ZnO nanostructures prepared in aqueous solution. Materials Letters. 62: 3099-3102.

Coleman, V. A. and Jagadish, C. 2006. Basic Properties and Applications of ZnO. *In* Zinc Oxide Bulk, Thin Films and Nanostructures. Jagadish, C. and Pearton, S., Ed. Elsevier Limited.

Connolly, J. R. 2007. Introduction to X-Ray Powder Diffraction. (online) Available http://epswww.unm.edu/xrd/xrdclass/01-XRD-Intro.pdf (31 June 2009)

Dutta, S., Chattopadhyay, S., Sutradhar, M., Sarkar, A., Chakrabarti, M., Sanyal, D. and Jana, D. 2007. Defects and the optical absorption in nanocrystalline ZnO. Phys.: Condens. Matter. 19: 236218.

Dutta, M., Midha, S. and Basak, D. 2008. Effect of sol concentration on the properties of ZnO thin films prepared by sol-gel technique. Applied Surface Science. 254: 2743-2747.

Fauteux, C., Smirani, R., Pegna, J., El Khakani, M. A. and Therriaul, D. 2008. Fast Synthesis of ZnO nanostructures by laser-induced chemical liquid deposition. Applied Surface Science.

Freepatentsonline. 2007. Zinc oxide based formulation for preventing and treating diarrhea in farm animals (online). Available http://www.freepatentsonline.com/EP1593381.html (15 October 2008)

GoldBamboo^{TM}. 2006. Zinc Oxide Cream, Ointment, and Paste (online). Available http://www.goldbamboo.com/topic-t4989-a1-6Zinc_Oxide.html

Goldstein, J., Newbury, D., Joy, D., Lyman, C., Echlin, P., Lifshin, E., Sawyer, L. and Michael, J. 2003. Scanning Electron Microscopy and X-Ray Microanalysis, 3rd, Springer Science.

Gupta, A., Bhatti, H. S., Kumar D., Verma, N. K., Tandon, R. P. 2006. Nano and bulk crystals of ZnO: synthesis and characterization. Digest Journal of Nanomaterials and Biostructures. 1: 1- 9.

Hammon, C. 1990. Introduction to Crystallography. Oxford University Press. Newyork. US.

Hi, P., Wei, Y., Lin, H. and Wang, X.-K. 2005. Growth of well-defined ZnO microparticles with additives from aqueous solution. J. Solid State Chem. 178: 855-860.

Holister. P., Weener, J.w., Vas, C.R., and Harper, T. 2003. Nanoparticles; Technology White Papers nn 3. Clientifca.

Hsiao, C.C., Huang, K.-Y. and Hu, Y.-C. 2008. Fabrication of a ZnO Pyroelectric Sensor. Sensors. 8: 185-192.

Hwangbo, S., Lee, Y.-J. and Hwang, K.-S. 2008. Photoluminescence of ZnO layer on commercial glass substrate prepared by sol–gel process. Ceramics International. 34: 1237–1239.

Jang, JM., Kim, SD., Chai, HM., Kim, JY., and Jang, WG. 2008. Morphology change of selfe assembled ZnO 3D nanostructures with different pH in the simple hydrothermal process. Mat. Chem. Phys. xxx-xxx (in-press).

Jiwei, Z., Liangying, Z. and Xi, Y. 2000. The dielectric properties and optical propagation loss of c-axis oriented ZnO thin films deposited by sol-gel process. Ceramics International 26: 883-885.

Joel, A. J. John J. H. Robert A. M. Paul M. B. Michael S. D. 2003. A multiple-scattering model analysis of zinc oxide pigment for spacecraft thermal control coatings. CAT.INIST (online). Available (http://cat.inist.fr/?aModele=afficheN&cpsidt=15369294)

Kim, G.-S., Ansari, S.-G., Seo, H.-K. Kim, Y.-S. Yang, O-B., H. –S, Shin. Hydrothermal growth of ZnO on annealed electrodeposited titanate film: Influence of zinc nitrate and methenamine. Applied Surface Science 253: 7197-7202.

Lee, J.-H., Ko, K.-H. and Park, B.-O. 2003. Electrical and optical properties of ZnO transparent conducting films by the sol–gel method. Journal of Crystal Growth. 247: 119-125.

Li, H., Wang, J., Liu, H., Yang, C. and Xu, H. 2004. Sol–gel preparation of transparent zinc oxide films with highly preferential crystal orientation. vacuum. 77: 57-62.

Li, H., Wang, J., Liu, H., Zhang, H. and Li, X. 2005. Zinc oxide films prepared by sol–gel method. Journal of Crystal Growth. 275: e943-e946.

Li, P. Liu, H., Zhang, Y.-F. Wei, Y. and Wang, X.-K. 2007. Synthesis of flower-like ZnO microstructures via a simple solution route Mater. Chem. And Phys. 106: 63-69.

Li, W.-J., Shi, E.-W., Zhoug, W.-Z. and Yin, Z.-W. J. 1999. Growth mechanism and growth habit of oxide crystals. Cryst. Growth. 203: 186-196.

Lu, C.-H., Lai, Y.-C. and Kale, R. B. 2008. Influence of alkaline sources on the structural and morphological properties of hydrothermally derived zinc oxide powders. Journal of Alloys and Compounds. xxx: xxx-xxx.

LUMINESCENCE SPECTROPHOTOMETER. LS55 Users Guide. 2000. Perkin Elmer Inc. UK.

Majumder, S.B., Jain, M., Dobal, P.S. and Katiyar, R.S. 2003. Investigations on solution derived aluminium doped zinc oxide thin films. Materials Science and Engineering B. 103: 16-25.

Mandal, S., Goswami, M.L.N., Das, K., Dhar, A.and Ray, S.K. 2008. Temperature dependent photoluminescence characteristics of nanocrystalline ZnO films grown by sol–gel technique. Thin Solid Films. 516: 8702-8706.

Mungkornasawakul, P., Rattanakit, N., Sirita, J., Plikomol4, A., Sripuan, T., Ounnunkad, S. and Phanichphant, S. 2005. ANTIMICROBIAL ZINC OXIDE NANOPOWDERS. 31st Congress on Science and Technology of Thailand at Suranaree University of Teachnology. 18-20 October 2005.

Nav Bharat Metalic Oxide Industries Pvt. Limited. 1978. Our company enjoys a highly diversified clientele. Some of the popular applications of Zinc Oxide are in the following industries: (online). Available http://navbharat.co.in/clients.htm (15 October 2008)

Northern Arizona University. 2006. Planetary Materials Microanalysis Facility (online). Available www4.nau.edu/.../Microprobe-SEM/Signals.html (24 October 2008)

O'Brien, S., Koh, L. H. K. and Crean, G. M. 2007. ZnO thin films prepared by a single step sol-gel process. Thin Solid Films. 516: 1391-1395.

OHBA Laboratory. (online) Available http://www.geocities.jp/ohba_ lab_ ob_ page/ Structure/ZnO_Wurtzite.jpg (19 October 2008)

Optional Accessories for Shimadzu UV-Vis spectrophotometers, Shimadzu corporation. International Marketing Division. Tokyo. Japan.

Pal, U. and Santiago, P. 2005. Controlling the Morphology of ZnO Nanostructures in a Low-Temperature Hydrothermal Process. J. Phys. Chem. B. 109: 15317-15321.

Qteish, A. 2000. Self-interaction-corrected local density approximation pseudopotential calculations of the structural phase transformations of ZnO and ZnS under high pressure. J. Phys.: Condens. Matter 12: 5639-5653.

Raoufi, D. and Raoufi, T. 2009. The effect of heat treatment on the physical properties of sol–gel derived ZnO thin films. Applied Surface Science. 255: 5812-5817.

Sagar, P., Shishodia, P.K., Mehra, R.M. 2007. Influence of pH value on the quality of sol–gel derived ZnO films. Applied Surface Science. 253: 5419-5424.

Sahal, M., Hartiti, B. Ridah, A., Mollar, M. and Mari, B. 2008. Structural, electrical and optical properties of ZnO thin films deposited by sol-gel method. Microelectronics Journal. 39: 1425-1428.

Samontha, A., Shiowatana, J. and Siripinyanond A. Elemental Size Characterization Of Cosmetic Products Using Sedimentation Field-Flow Fractionation With Inductively Coupled Plasma-Mass Spectrometry. Department of Chemistry. Faculty of Science. Mahidol University: Rama 6 Road. Bangkok. Thailand.

Scintag, Inc.1999. Chapter 7: Basics of X-ray Diffraction (online). Available http://epswww.unm.edu/xrd/xrdbasics.pdf (15 October 2008)

Serpone, N., Lawless, D. and Khairutdinov, R.1995. Size Effects on the Photophysical Properties of Colloidal Anatase TiO_2 Particles: Size Quantization versus Direct Transitions in This Indirect Semiconductor. J. Phys. Chem. 99: 16646-16654.

Serrano, J., Romero, A.H., Manjon, F.S., Lauck, R. Cardona, M. And Rubio, A. 2004. Pressure dependence of the lattice dynamics of ZnO: An *ab initio* approach. Physical Review B. 69, 094306: 9.

Sobana, N. and Swaminathan, M. 2007. The effect of operational parameters on the photocatalytic degradation of acid red 18 by ZnO. Separation and Purification Technology. 56: 101-107.

Sun, G. Cao, M, Wang, Y., Hu, C., Liu, Y., Ren, L. and Pu, Z. 2006. Anionic surfactant-assisted hydrothermal synthesis of high-aspect-ratio ZnO nanowires and their photoluminescence property. Mater. Lett. 60: 2777-2782.

The University of New Mexico. 2008. (online) Available http://www.mtsc.unt.edu /FACULTY/ bgorman/3020/3020%20Lecture%208%20-%20XRD.pdf (15 October 2008)

Tsay, C.-Y., Cheng, H.-C., Tung, Y.-T., Tuan, W.-H. and Lin, C.-K. 2008. Effect of Sn-doped on microstructural and optical properties of ZnO thin films deposited by sol–gel method. Thin Solid Films. xx: xxx- xxx.

U.S. Geological Survey. 2008. (online). Available http://pubs.usgs.gov/of/2001/of01-041/htmldocs/images/xrdtube.jpg (30 October 2008)

Vafaee, M. and Ghamsari, M.S. 2007. Preparation and characterization of ZnO nanoparticles by a novel sol–gel route. Materials Letters. 61: 3265-3268.

Valeur, B. 2002. Molecular Fluorescence: Principles and Applications. Wiley VCH. German.

Wang, H., Xie, C. Zhang, W., Cai, S., Yang, Z. and Gui, Y. 2007. Comparison of dye degradation efficiency using ZnO powders with various size scales. Journal of Hazardous Materials. 14: 645–652.

Weller, M.T. 1996. Inorganic Material Chemistry. Oxford Chemistry Primer.Oxford Science Publication. Grate Britain. England.

Wikimedia Common. 2009. File: Bragg diffraction.png. (online) Available http://commons.wikimedia.org/wiki/File:Bragg_diffraction.png (31 June 2009)

Wikimedia Foundation, Inc. 2008. Zinc oxide (online). Avaliable http://en.wikipedia.org/wiki/zinc-oxide (15 October 2008)

Wikimedia Foundation, Inc. 2008. Ethanolamine (online). Available http://en.wikipedia.org/wiki/File:Ethanolamine-2D-skeletal-B.png (24 June 2009)

Wikimedia Foundation, Inc. 2008. Diethanolamine (online). Available http://en.wikipedia.org/wiki/File:Diethanolamine.png (24 June 2009)

Wikimedia Foundation, Inc. 2008. Triethanolamine (online). Available http://en.wikipedia.org/wiki/File:Triethanolamine.png (24 June 2009)

Wikimedia Foundation, Inc. 2008. Scanning electron microscope (online) Available http://en.wikipedia.org/wiki/Scanning_electron_microscope10/11/2008 (15 Octorber 2008)

Winfield, R.J., Koh, L.H.K., O'Brien, S. and Crean, G. M. 2007. Excimer laser processing of ZnO thin films prepared by the sol–gel process. Applied Surface Science. 254: 855-858.

Wu. C., Qiao, X., Chen, J., Wang, H., Tan, F. and Li, S. 2006. A novel chemical route to prepare ZnO nanoparticles. Mater. Lett. 60: 1828-1832.

Xie, R., Li, D., Zhang, H., Yang, D., Jiang, M. Sekiguchi, T., Liu, B. and Bando, Y. 2006. Low-Temperature Growth of Uniform ZnO Particles with Controllable Ellipsoidal Morphologies and Characteristic Luminescence Patterns. J. Phys. Chem. B. 110: 19147-19153.

Xinshu, N., Weiping, D. and Weimin, D. 2004. Preparation and gas sensing properties of ZnM_2O_4 (M = Fe, Co, Cr).Sensor and Actuators B. 99: 405-409.

Xu, J., Pan, Q., Shun, Y. and Tian, Z.2000. Grain size control and gas sensing properties of ZnO gas sensor. Sensors and Actuators B. 66: 277-279.

Xu, S., Li, Z.-H., Wang, Q. Cao, L.-J., He, T.-M. and Zou, G.-T. 2008. A novel one-step method to synthesize nano/micron-sized ZnO sphere. Journal of Alloys and Compounds 465: 56-60.

Xue, S.W., Zu, X.T., Shao, L.X., Yuan, Z.L., Zheng, W.G., Jiang, X.D. and Deng, H. 2008. Effects of annealing on optical properties of Zn-implanted ZnO thin films. Journal of Alloys and Compounds. 458: 569-573.

Yahia, S. B., Znaidia, L., Kanaeva, A. and Petitet, J.P. 2008. Raman study of oriented ZnO thin films deposited by sol–gel method. Spectrochimica Acta Part A. 71: 1234-1238.

Yu, K., Jin, Z., Liu, X., Zhao, J. and Feng, J. 2007. Shape alterations of ZnO nanocrystal arrays fabricated from $NH_3 \cdot H_2O$ solutions. Applied Surface Science 253:4072-4078.

VITAE

Name   Miss Kanokwan   Thongsuriwong

Student ID   5010220001

Educational Attainment

Degree	Name of Institution	Year of Graduation
B. Ed. (Science-Chemistry)	Thaksin University	2006

Scholarship Awards during Enrolment

Center of Excellence for Innovation in Chemistry Commission on Higher Education, (PERCH-CIC)

Teaching Assistant, Department of Chemistry, Prince of Songkla University

List of Publication and Proceedings

Thongsuriwong, K., Amornpitoksuk, P. and Suwanboon, S. 2009. The effect of aminoalcohols (MEA, DEA and TEA) on morphological control of nanocrystalline ZnO particles. Proceeding of the 12th National Graduate Research Conference co-organized by CGAU and Khon Kaen University, Khon Kaen, Thailand, 12-13 February 2009. pp. 751-756.